Master's thesis

2019

Li Li

Master's thesis

NTNU
Norwegian University of
Science and Technology
Faculty of Engineering
Department of Civil and Environmental Engineering

Li Li

Hydrological modelling of grey roof during winter: Case study of a pilot project in Trondheim

June 2019

NTNU
Norwegian University of
Science and Technology

NTNU
Norwegian University of
Science and Technology

NTNU

Norwegian University of
Science and Technology

Hydrological modelling of grey roof during winter: Case study of a pilot project in Trondheim

Li Li

Civil and Environmental Engineering
Submission date: June 2019
Supervisor: Sveinung Sægrov, IBM
Co-supervisor: Vladimir Hamouz, IBM
Per Møller-Pedersen

Norwegian University of Science and Technology
Department of Civil and Environmental Engineering

Abstract

Climate change has brought stormwater problems, while at the same time urbanization has also changed most of permeable surface in urban area to impermeable road, parking lots and residential area. These have led to big challenge to the urban drainage system. In order to resolve the stormwater problem, many institutions have put effort on developing new tools for dealing with the stormwater in different phases.

Klima 2050 has conducted several projects concerning managing stormwater in early phase in urban area. One of the solutions is nature-based rooftop retrofitted from conventional black roof, for example blue-green and blue-grey roofs. One study has shown great detention capacities and some retention performance during warm seasons by the pilot grey roof located at Høvringen in Trondheim, Norway. However, hydrological performance during colder seasons with snow on the rooftop and frozen aggregate is less familiar. In order to obtain more concrete knowledge about the pilot grey roof especially during winter, this master thesis will focus on event-based analysis and hydrological modelling of the roof to explain impacts of cold weather on the water handling performance.

The research period was set from 1st Dec 2017 to 15th Apr 2018. Eight events with large amount of runoff were chosen for the analysis of hydrological performance. It was common to include retention (capacity to permanently hold water) and detention (ability to postpone and attenuate the peak from an event) into consideration. Furthermore, in order to simulate runoff from the grey roof, a conceptual model was set up based on three well-founded models: snow process by energy balance method, ice-water phase change and modelling for underlying substrate. A model built in EPA SWMM was used on the purpose of comparison of simulations against the conceptual model. Calibration of the two models followed the research period. Simulation results after the calibration was assessed by Nash-Sutcliffe Efficiency (NSE) and Relative Percentage Difference (RPD) of Volume.

Event-based analysis demonstrated that the grey roof was able to attenuate 34.62% in average of peak flows ranging from -20.44 to 82.26% quantitatively, and delay the peak flow for 12 hours and 10 minutes in average ranging from -21 h 29 min to 73 h 05 min. It was during snowmelt events that became extremely difficult to predict peaks as it could bring forward or enlarge the peak flow, making the performance even worse than that on conventional roofs.

The conceptual model achieved NSE of 0.84 and RPD of -3.1% in contrast to SWMM with NSE of 0.39 and RPD of -7.1%. Simulated runoff by the conceptual model turned out to be the best representative of observed runoff. But through the event-based analysis it was found that larger runoff events had obtained better simulations than that in smaller events. Due to the low accuracy and improper estimation of snow process (partial energy balance), SWMM failed to follow minor changes in runoff and peaks. Simulated snow depth by the conceptual model showed also good correlation to the snow condition recorded by camera on the roofs. Since data for example snow depth, ice content and initial conditions was not provided, further improvement of the conceptual model became difficult for the current work. Despite of time limitation and site-specific problem, the conceptual model was still to some extent able to explain the water routine from precipitation to runoff. It was also very promising for improvements of the conceptual model for runoff predictions from the grey roof.

Sammendrag

Klimaendringene har medført overvannsproblemer. Samtidig har urbaniseringen også forandret den meste parten av permeable overflaten i byområdet til tett overflate for eksempel vei, parkeringsplasser og boligområde. Disse har satt stor utfordring for urbane dreneringssystemet. For å løse overvannsproblemet har mange institusjoner lagt vekt på å utvikle nye løsninger for å håndtere overvannet i ulike faser.

Klima 2050 har gjennomført flere prosjekter for å håndtere overvann i tidlig fase i byområdet. En av løsningene er naturbasert tak som er ettermontert fra konvensjonelt tak, for eksempel blågrønne- og blågråetak. En artikkel har vist stor vannforsinkelses-kapasitet og noe lagringskapasitet i varme årstiden av pilot gråetaket lokalisert på Høvringen i Trondheim. Men hydrologiske ytelser i kaldere tid med snø på taket og frossent underlag er mindre kjent. For å få mer fagkunnskap om pilot gråetaket spesielt om vinteren, skal denne masteroppgaven fokusere på hendelsesbasert analyse og hydrologisk modellering av taket.

Forskningsperioden ble satt fra 1. desember 2017 til 15. april 2018. Åtte hendelser med stor mengde avrenning ble valgt for å analysere hydrologiske ytelsene. Det var rimelig å inkludere lagringskapasitet og fordrøyningskapasitet. Videre ble det opprettet en konseptmodell for å simulere avrenningen fra gråetaket. Modellen var bygget opp på tre modeller: snø prosess ved energibalanse metoden, is-vann fase endring og modellering for underlaget. En modell i EPA SWMM var brukt for å sammenligne simulert avrenningen med konseptmodellen. Kalibreringsperioden var også forskningsperiode. Simuleringsresultater etter kalibreringen ble vurdert ved NSE og RPD of Volume.

Analysen fra hendelsene viste at gråetaket kunne redusere den største avrenningen ved 34,62% i gjennomsnitt (fra -20,44 til 82,26%), og forsinket den største avrenningen i 12 timer og 10 minutter i gjennomsnitt (fra -21 t 29 min til 73 t 05 min). Det var under snøsmelting hendelser som ble ekstremt vanskelig å profetere om den største avrenningen da en større største avrenningen kunne forekomme på forskudd. Dette har gjort overvannshåndtering enda verre enn det på vanlige tak.

Den konseptuelle modellen oppnådde NSE på 0,84 og RPD på -3,1% i motsetning til SWMM med NSE på 0,39 og RPD på -7,1%. Simulerte avrenningen av konseptmodellen viste seg å være den beste representanten for observerte avrenningen. Men gjennom forskningshendelsene ble det funnet at hendelsene med større avrenning hadde fått bedre simuleringer ved konseptmodellen enn dem som har mindre avrenning. På grunn av lav oppløsning og uegnete metoden for snø prosessen (delvis energibalanse), klarte ikke SWMM å følge fluktuasjoner av avrenningen. Simulerte snødybden ved konseptmodellen viste også god korrelasjon til snøforhold registrert av kamera på taket. Siden data for eksempel snødybde, ismengde og initialbetingelse ikke ble gitt, ble ytterligere forbedringen av konseptmodellen vanskelig for dagens arbeid. Til tross for tidsbegrensning og stedsspesifikke problem, evnet konseptuelle modellen å beskrive til en viss grad vannprosessen fra nedbør til avrenning. Det var også veldig lovende for forbedringer for å profetere om hydrologiske ytelsene til gråetak.

Preface

The thesis is submitted to the Norwegian University of Science and Technology (NTNU), Department of Civil and Environmental Engineering. It is a product of the subject TVM4905 – Water Supply and Wastewater Systems, Master's Thesis. The thesis aims at assessing hydrological performance of a pilot grey roof located at Høvringen, Trondheim during the winter period 2017-2018, and establishing a conceptual model of the grey roof to simulate runoff from the roof.

First of all, a much thanks to my supervisor Professor Sveinung Sægrov and co-supervisors PhD candidate Vladimir Hamouz, General Manager of Storm Aqua AS Per Møller-Pedersen. Sveinung Sægrov played an important role as the coordinator between theoretical knowledge and practical experience, and supported with concrete suggestions to the structure of the thesis. Vladimir Hamouz contributed so much to the ideas of the thesis, and anticipated in several interesting lab tests. Without his effort the work would have become boring and difficult to be implemented. Per Møller-Pedersen took me to the factory where manufacture of grey roofs was implemented, and provided with valuable research data.

A special thanks to Researcher Jardar Lohne who assisted with the writing and Tone Merete Muthanna who provided an opportunity to present the product to more experts within the field. More thanks to my family and friends who have helped and inspired me during the half year.

Trondheim, June 10, 2019

Li Li

Li Li

Thesis Structure

The master thesis is written in the form of a scientific article and about to submit to *Journal of Water.* Main content of the thesis is the manuscript of the article.

Some appendixes are part of the master thesis, and Matlab code used for implementing the conceptual model is attached in Appendix 5.

Table of Contents

List of Figures

List of Tables

List of Abbreviations

ATI	Antecedent Temperature Index
CM	Conceptual Model
FC	Field Capacity
HC	Hydraulic Conductivity
LECA	Light Expanded Clay Aggregate
LID	Low Impact Development
NSE	Nash-Sutcliffe Efficiency
RPD	Relative Percentage Difference
SD	Snow Depth
SWMM	Storm Water Management Model
TP	Time Point

Hydrological modelling of grey roof during winter: Case study of a pilot project in Trondheim

Li Li

Department of Civil and Environmental Engineering, The Norwegian University of Science and Technology (NTNU), 2019

Abstract

The frequent stormwater events due to climate change have led to the application of grey and green roofing in urban areas. Although their water management performance has been studied under numerous climate conditions, the effects of snow and freezing substrates on these roofs is not well understood. This study aims at first creating a conceptual model for grey roofing in Trondheim during the winter period and then discussing various impacts of freezing weather on its hydrological performance.

Retention and detention capacities were assessed throughout one winter season that saw several runoff events. A conceptual model was also established on the basis of well-founded knowledge: the snow process described by using an energy balance method, the ice-water phase changes and modelling for the underlying substrate. An EPA SWMM model was utilized for the purpose of comparing with the conceptual model.

A 34.62% (average) quantitative peak attenuation and a 12 h and 10 min time delay were observed via event-based analysis. The calibrated conceptual model achieved a simulation result with a Nash-Sutcliffe Efficiency reading of 0.84 in contrast to SWMM's reading of 0.39, having improved simulations for larger runoff events. At last, grey roofing was able to contribute to milder runoff during winter.

Despite of time and site limitations from the conceptual model, it is still able to describe water patterns, a feature which may be used for making predictions.

Key words

Hydrological performance, LECA, energy balance method, frozen substrate, conceptual model

1 Introduction

Urbanization and climate change have produced a charged global discussion concerning stormwater management in urban areas. It is not surprising that roofing accounts for up to 40-50% of impermeable surface areas of building construction in most developed cities [1]. An increasing number of floods are affecting humans and causing natural disasters around the world. At the same time, old drainage systems and solutions are no longer able to handle this dramatic flow increase. Fortunately, instead of collecting and transporting all stormwater from the city to recipients by pipes, the idea of dealing with stormwater at an early phase (the first step of three-step stormwater treatment trains in Norway [2]) cannot only reduce the total amount of water and peak flow but also postpone peak time in an effective way. Grey roofing, also described as the application of a permeable paver having a lightweight, expanded clay aggregate (LECA)-based rooftop, is an example. Moreover, the pilot grey roof in Trondheim has achieved an excellent performance level as regards attenuation of peak flow; it also has a certain level of water-holding capacity and peak delay [3].

Spring snowmelt runoff is one of the issues that challenge urban drainage systems, even though one research study showed a decrease in snow's depth and coverage in some regions due to global warming [4]. Another study indicated even greater direct runoff during spring flooding than the one during summer [5]. For instance, severe spring snowmelt flooding has taken place in urban areas of both Sweden and Norway [6,7]. A high rate of snow melt , compacted soil, and rain on snow events have contributed to large runoff intensity in several cities [8]. Moreover, cold weather in Norway during the winter seasons induces freezing and thawing in the soil and underlying substrate. Volume expands when liquid water freezes, which creates smaller pore spaces in frozen soil [9]. Thus, the infiltration capacity is weakened [10], and larger portions of water from either rainfall or snowmelt form overland flow [11]. Three incidents of bioretention have been studied in Norway, and it has been found that saturated hydraulic conductivity of these bioretention during winter has become more than halved compared to that during summer [12]. All of these warnings indicate that the problem of stormwater management in late winter and early spring should be resolved properly.

The hydrological process during winter is complex, as snow may accumulate on roofs and ice freezes in the substrate. The snow process may be simulated by several types of software [13,14] in which two approaches are applied most often: 1) energy balance method and 2) degree day method. In addition, these approaches have achieved fairly good simulations in comparison with the observed data [15-19]. The energy balance model is more suitable for open areas having a dramatic variability of climatic conditions when sufficient data source is accessible [20]. The method includes radiation, sensible and latent heat, convective heat from rainfall and ground heat. A total net of incoming heat to snow causes melting, whereas the meltwater is stored until the water content reaches the free water-holding capacity of snow. The capacity is a function of snow water equivalent to the snow pack [15]. Redundant water from the snow pack infiltrates into the substrate. There are many tools for modelling water balance in the substrate of blue-green infrastructures, including grey and green roofs, and raingardens [21]. A simple but effective conceptual model for green roofs has been proposed [22-24]. The conceptual model consists of a surface submodule, a subsurface submodule and a drainage submodule. Interception and

evapotranspiration play the most important roles in water balance on the surface. The wilting point, field capacity, saturated capacity and infiltration rate determine the infiltrated water's patterns in the subsurface submodule. Further, saturated hydraulic conductivity is necessary for calculating flow in drainage layers when using Darcy's law. Water flow in frozen substrate is common during winter in cold climates. However, infiltrated water's pattern is complicated because of the ice-water phase change. In order to resolve this problem, a one-dimensional energy conservation equation for estimating water flow in frozen soil was applied [25,26].

The EPA Storm Water Management Model (SWMM) equipped with Low Impact Development (LID) control has already been applied to several different scales of green/grey roofs for warm seasons, achieving positive results using Nash-Sutcliffe Efficiency (NSE) and varying from 0.44 to 0.93 [27-29]. Unfortunately, no wintertime research results about SWMM (with the presence of snow and ice in the substrate) has been found. This study will try to estimate the simulation performance of EPA SWMM for one winter period in a cold climate.

Klima 2050 is an innovation research center in Norway whose aim is to promote innovative solutions and knowledge concerning how to adapt to climate change [30]. The research center has built up a pilot grey roof at Høvringen in Trondheim, and this rooftop is used for analyzing stormwater management. Trondheim is situated at 63º N, and the average monthly temperature from November - February is below +1 ℃ [3]. The largest snow accumulation there in 2018 was measured at 25 cm by Voll meteorological station [31]. The presence of snow on the rooftops and frost on the ground usually lasts for several months each winter.

The article's main objective is to fill in the gaps of knowledge regarding the grey roof's hydrological performance during winter and apply the conceptual green roof model to the grey roof. In order to fulfil this objective, modelling the snow process and ice-water phase change must also be considered. Thus, a conceptual model (CM) simulating precipitation to runoff has been established. Based on this objective, three research questions have been formulated:

1. How effective is the event-based hydrological performance of the grey roof during winter in a cold climate?
2. How effective is the performance of the CM and SWMM for both long-term continuous and event-based simulations of the grey roof during winter?
3. What are limitations and applications of the CM?

2 Material and Method

2.1 Description of the pilot grey roof

The article's research subject is lightweight expanded clay aggregate (LECA)-based grey roofing located at the Høvringen wastewater treatment plant in Trondheim, Norway, which was constructed in November 2016 (Figure 2.2). Trondheim (Figure 2.1) is located in the central region of Norway and has a maritime temperate climate [32]. The weather in Trondheim is generally considered to be unstable, with heavy rainfall (850mm per year), short summers and long, snowy winters [3,32].

The grey roofing consists of three layers: top-layer concrete pavers comprised of 200 mm thick crushed LECA substrate, protective geotextile and asphalt waterproofing membrane on the bottom, as shown in Figure 2.3. Gaps between each paver block allow large amounts of water to infiltrate through the roof. The crushed LECA has a particle distribution of 1.5-2.5mm. Based on lab tests, additional substrate properties include having a bulk density of 500 kg/m3, porosity of 55% and field capacity (FC) of 20.4%. The total precipitation area is $100m^2$ with the substrate-covered central roofing part accounting for $88m^2$.

A camera was set to record images of the three roofs once every hour. Throughout the entire winter of 2017-2018, the first big snowfall was recorded by the camera from the morning of 3 December 2017 to the last fusion in the afternoon of 12 April 2018.

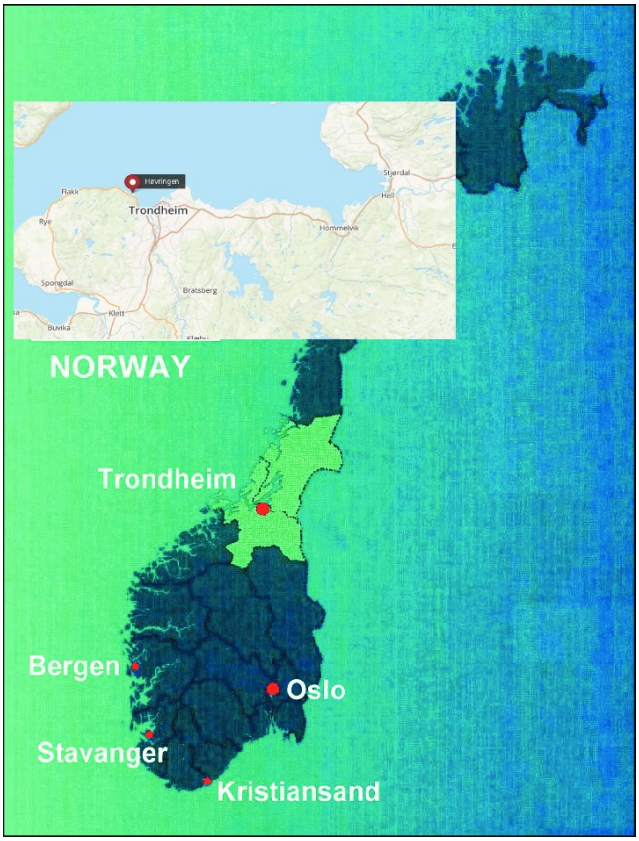

Figure 2.1. Location of Høvringen in Trondheim, Norway [33,34].

Figure 2.2. A full-scale view of the pilot grey roof (closest) together with black conventional (reference) roof (middle) and green roof (furthest).

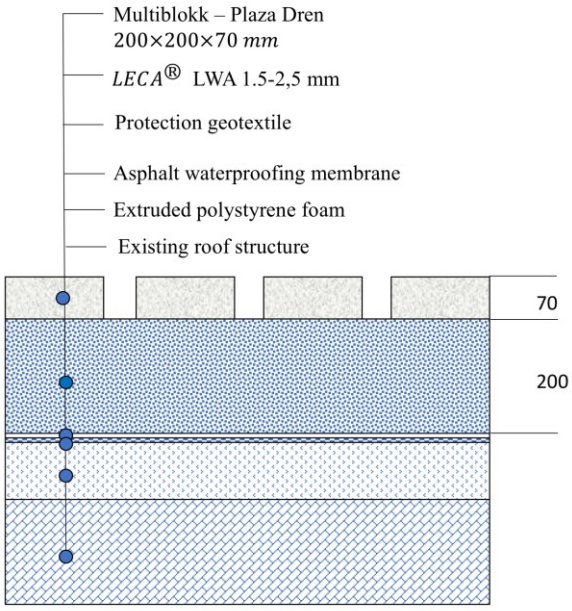

Figure 2.3. Configuration of the grey roof from cross-section, consisting of three layers: Top pavers, underlying Leca and water-proof layer.

2.2 Meteorological data

A heated, rain gauge bucket was installed 5 meters above the grey roof that measured the precipitation [mm], humidity [%] temperature [℃], and solar radiation [W/m^2]. The wind speed [m/s] was measured using an anemometer placed 2 meters above the roof. Two soil moisture sensors (Decagon devices) were inserted into the roof in order to measure permittivity levels in the substrate. The calibration between the water content and permittivity was mathematically completed through lab tests. These two sensors could also measure the temperature. A single thermal sensor was placed at the bottom of the roof. The flow from the roof was collected by two tanks located inside the building. The weighing of both the tank and water proceeded continuously. Thus, the weight of runoff from the roof was calculated as well as its corresponding volume. A central CR1000 data logger recorded the data at 1-minute intervals.

2.3 Observed hydrological performance and research period

Hamouz and Johannessen [2,3] studied green and grey roofing at several locations in Norway, and the research periods varied from several months to 8 years in length. The hydrological performance of these roofs refers to common retention capacity (long-term analysis) and detention capacity (event-based). Retention capacity is the roof's permanent water-retaining capacity that is affected by climate, vegetation type, property and depth of the underlying substrate. Detention capacity describes a roof's ability to postpone and attenuate the peak during a precipitation event. The antecedent dry period, total precipitation amount and intensity as well as hydraulic conductivity (HC) play important roles in detention. In order to evaluate the hydrological performance during the research period between 1 December 2017 and 15 April 2018, eight events having large amounts of runoff were chosen. The characteristics of each event are shown in Table 2.1. A precipitation event starts with an antecedent time of at least 6 hours [2]. The event type *mix* is defined as rain followed by rain and snow. Lastly, the impact of rainfall on snowmelt during events 6 and 8 has been left out.

Event	**Type**	**Duration**	**Total precipitation**	**Average intensity**
		(hh:mm)	**(mm)**	**(mm/hr)**
1	Mix	62:50	45.7	0.73
2	Mix	28:40	23.00	0.80
3	Rain on snow	149:35	61.80	0.41
4	Rain on snow	8:17	4.40	0.53
5	Mix	95:44	32.20	0.34
6	Snowmelt	67:49	/	/
7	Snow	11:01	10.30	0.94
8	Snowmelt and Thawing	231:23	/	/

Table 2.1. Characteristics of all events during the research period.

2.4 Introduction of the CM

The CM consisted of a snow pack model, ice-water phase change model and modelling for underlying aggregate, see Figure 2.4. Details may be described in the following manner:

1. Temperatures that differentiated snowfall and rainfall: It was assumed that total precipitation fell as rain above an air temperature of T_{max} (℃), and snow below T_{min} (℃). The amount of rain and snow was obtained by interpolation of air temperature in between [17]:

$$\mathrm{P_{snow}} = \frac{\mathrm{T_{max} - T_a}}{\mathrm{T_{max} - T_{min}}} * \mathrm{P_{total}}, \quad (1)$$

   where $P_{rain} = P_{total} - P_{snow}$. $\mathrm{P_{prec}}$ is the total amount of precipitation in [mm]. $\mathrm{P_{snow}}$ is the amount of snowfall in water equivalent [mm], $\mathrm{P_{rain}}$ is the amount of rainfall in [mm]. T_{max} and T_{min} were decided around 1.5℃ and 1.2℃ respectively upon analyzing the recorded pictures and measured air temperature.

2. Snow pack model (2.4.1): The snow pack's temperature was set to 0 ℃ when the air temperature was positive and equal to the air temperature when negative. Water exceeding the free water holding capacity ran off and infiltrated into the grey roof.
3. Ice-water phase change (2.4.3): The process was derived from the one-dimensional energy conservation equation. Derivation was given in Appendix 1.
4. Modelling for underlying substrate (2.4.4): The actual water content level was determined after the ice-water phase change process. The simulated flow was obtained by applying Darcy's law [26].
5. Calibration (2.6).

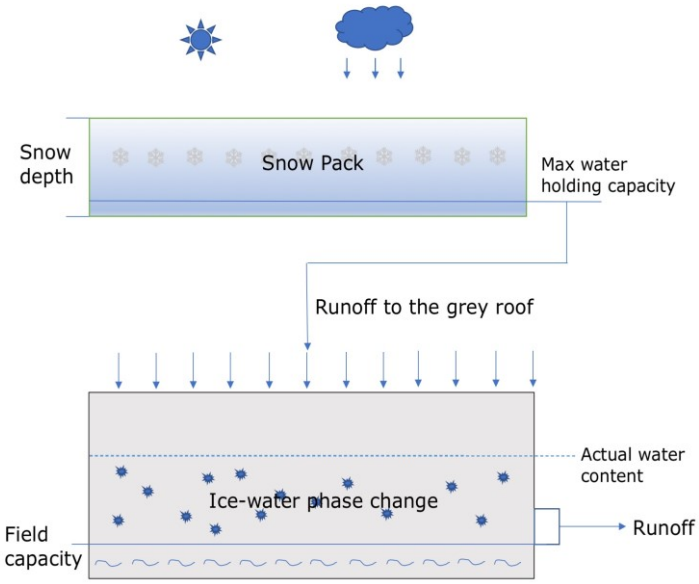

Figure 2.4. An overview of simulation process by the conceptual model.

2.4.1 Snow process by energy balance method

The equation derived by applying the one-dimensional energy conservation equation is given below, where ground heat is not considered:

$$\mathrm{Q_{total}} = \mathrm{Q_{net,sw}} + \mathrm{Q_{net,lw}} + \mathrm{Q_e} + \mathrm{Q_s} + \mathrm{Q_{conv}}, \quad (2)$$

Where Q_{total} is the total incoming energy absorbed by ($Q_{total} > 0$) or released from ($Q_{total} < 0$) the snow pack; $Q_{net,sw}$ is the net incoming shortwave radiation; $Q_{net,lw}$ is the net incoming longwave radiation; Q_e is latent heat; Q_s is sensible heat, and Q_{conv} is convective heat from rainfall. All terms are in $[W/m^2]$.

2.4.1.1 Shortwave radiation

Shortwave radiation is the solar radiation; Smooth, white snow on roofs is able to reflect most shortwave radiation:

$$\mathrm{Q_{net,sw}} = \mathrm{Q_{ir}} * (1 - \gamma), \quad (3)$$

Q_{ir} is the total incoming solar radiation (W/m^2); γ is snow albedo, 0.9 for deep and fresh snow, which is assumed to decrease in accordance with the snow depth [35].

2.4.1.2 Longwave radiation

The Stefan-Boltzmann law provides a universal formula for net longwave radiation.

$$\mathrm{Q_{net,lw}} = \varepsilon_a \sigma \mathrm{T_a} - \varepsilon_s \sigma \mathrm{T_s}, \quad (4)$$

σ is the Stefan-Boltzmann constant, $5.67 * 10^{-8}\, W/m^2 \cdot K^4$, ε_a is the emissivity from the atmosphere, ε_s is the emissivity of snow pack: 0.98 [36], T_a is the air temperature [℃], and T_s is the snow pack's temperature.

Emissivity from the atmosphere ε_a is proposed as $(\frac{1-Q_{ir}/Q_{xx}}{3.82} * (0.74 + 0.0049 e_a))$ when there is positive solar radiation, and $(0.09 + 0.0059e)$ when there is none [17].

Q_{xx} is extraterrestrial shortwave radiation and can be estimated by [37]:

$$\mathrm{Q_{xx}} = 1366.1 * (1.00011 + \left(0.034221 * \cos\left(2\pi * \frac{\mathrm{N}}{365}\right)\right) + \left(0.00128 * \sin\left(2\pi * \frac{\mathrm{N}}{365}\right)\right) + \left(0.000719 * \cos\left(\pi * \frac{\mathrm{N}}{365}\right)\right) + (0.000077 * \sin(\pi * \frac{\mathrm{N}}{365}), \quad (5)$$

N is the day number of the year.

e_a is the air vapor pressure in millibars (mb) [38]:

$$\mathrm{e_a} = \mathrm{RH} * \left(1.0007 + (3.46 * 10^{-6}\mathrm{P})\right) * 6.1121 \mathrm{e}^{\frac{17.502\mathrm{T_a}}{240.97+\mathrm{T_a}}}, \quad (6)$$

P is the atmosphere 10^5 Pa; RH is relative humidity.

2.4.1.3 Latent heat

Heat exchanges between the snow pack and atmosphere due to condensation or fusion at a constant temperature is called latent heat. It is calculated by [15]:

$$\mathrm{Q_e} = 2359.9 * 8.5 * 0.673 * 2.24 (\mathrm{z_t z_b})^{-\frac{1}{6}} \mathrm{U_b} (\mathrm{e_a} - \mathrm{e_s}), \quad (7)$$

z_t and z_b are heights above the roof of temperature and wind sensors, and factor 0.673 converts feet to meters; U_b is the wind speed, and factor 2.24 converts miles/hr to m/s; e_s is the saturation vapor pressure on the snow surface (mb) and is estimated as [38]:

$$e_s = \left(1.0003 + (4.18 * 10^{-6} P)\right) * 6.1115 e^{\frac{22.452 T_a}{272.55 + T_a}}, \quad (8)$$

2.4.1.4 Sensible heat

Sensible heat is the energy transfer when the snow pack is heated up or cooled down by air temperature, and may be calculated by [15]:

$$Q_s = \gamma * \frac{T_a - T_s}{e_a - e_s} * Q_e, \quad (9)$$

γ is the psychometric constant ($mb/℃$) (0.00057 P_a).

2.4.1.5 Convective heat from rainfall

Rain on snow is one of the most important factors that accelerates snowmelt:

$$Q_{ad} = C_w P_{rain} (T_a - T_m), \quad (10)$$

where C_w is the specific heat capacity of water, 4.8 kJ/kg·K; and T_m (0℃) is the melting temperature for snow.

2.4.1.6 Heat exchange between the outside, snow and water

A net amount of positive incoming heat ($Q_{total} > 0$) heats up the snow pack so that it starts to melt:

$$Q_m = \min(0, -(Q_{total} - c_s \rho_w D_{snow} * (T_o - T_s))), \; Q_{total} > 0, \quad (11a)$$

$$\Delta_{water} = P_{rain} - \max(\frac{Q_m}{\rho_w \lambda_{snow}}, -D_{snow}), \quad (11b)$$

$$\Delta_{snow} = P_{snow} + \max(\frac{Q_m}{\rho_w \lambda_{snow}}, -D_{water}), \quad (11c)$$

Q_m is the heat exchange between snow and its contained water; Δ_{water} and Δ_{snow} are the changes in water and snow in [mm] at this point in time ; ρ_w is the water density (1000 kg/m^3); λ_{snow} is the latent fusion heat for snow (333.6 kJ/kg); D_{snow} and D_{water} are the depths of snow and water [mm] respectively during this time sequence.

Negative incoming heat enters prior to refreezing water in the snow pack:

$$Q_m = \min(-Q_{total}, \rho_w \lambda_{snow} D_{water}), \text{ if } Q_{total} < 0, \quad (11d)$$

$$\Delta_{water} = P_{rain} - \min(\frac{Q_m}{\rho_w \lambda_{snow}}, D_{snow}), \quad (11e)$$

$$\Delta_{snow} = P_{snow} + \min(\frac{Q_m}{\rho_w \lambda_{snow}}, D_{water}), \quad (11f)$$

2.4.2 Infiltrated water

The amount of runoff [mm] on the grey roof is determined by the following:

$$q_{inf} = D'_{water} - D_{water} * Fr, \quad (12)$$

where D'_{snow} and D'_{water} are the snow and water depths in the next time sequence in [mm]; Fr [%] is the snow pack's maximum water holding capacity , and ranges from 0.02-0.25 [15].

2.4.3 Ice-water phase change

With the exception of the final two sequences from the energy conservation equation, it has also been observed that the snow pack played an important role as an insulation layer between the grey roof and surrounding atmosphere. When snow was shallow, the phase change was highly dependent upon air temperature fluctuations. Therefore, the sensible heat of air Q_{sa} has also been considered:

$$\mathrm{Q_{total}} = \mathrm{Q_{ad,sub}} + \mathrm{Q_{ad,water}} + \mathrm{Q_{sa}}, \tag{13a}$$

$$\mathrm{Q_{ad,sub}} = \mathrm{C_{leca}}(\mathrm{T_{sub}} - \mathrm{T_f}), \tag{13b}$$

$$\mathrm{Q_{ad,water}} = \mathrm{C_w q_{inf}}(\mathrm{T_{inf}} - \mathrm{T_f}), \tag{13c}$$

$$\mathrm{Q_{sa}} = \mathrm{C_{air}}(\mathrm{T_a} - \mathrm{T_f}), \mathrm{if\ D_{snow}} < 0.5\mathrm{mm}\ ;\ \mathrm{else\ Q_{sa}} = 0, \tag{13d}$$

Where C_{leca} is the heat capacity of LECA; T_{sub} is the temperature in the substrate; T_f is the freezing temperature of ice, observed to be -0.15℃ in LECA; T_{inf} is the temperature of infiltrated water, equivalent to 0℃ if snowmelt water and T_a if rainfall.

2.4.4 Modelling for underlying substrate

The 1.5-2.5mm LECA has large particle sizes and fairly uniform distribution, which makes this fall within the 1-minute resolution time during which water is able to reach the drainage sub-module. FC of the LECA substrate has been determined by observed permittivity, 0.18. The difference, when compared to the lab test, results from the errors of calibration process between calculated water content and measured permittivity:

$$\mathrm{q_{total}} = \mathrm{KA}\cdot\sin\omega\ , \tag{14}$$

where q_{total} is the total runoff from the grey roof [l/min]; K is HC in [m/min], and it is believed that HC varies in the presence of ice; A is the cross-section area regarding actual water content [m^2]; ω is the slope of 0.02, and $sin\omega$ is the hydraulic gradient.

2.4.5 Initial conditions and assumptions

At the outset, the model must meet certain conditions. For instance, in the case of the snow pack, the initial SD is set at 0 mm. Due to the fact that the moisture sensor fails to physically measure ice content and detect water content in cold weather, both the initial water content (0.09) and ice content (0.15) have to be calibrated.

In addition, more assumptions have been put forward in order to optimize the CM:

- A considerably small amount of average evapotranspiration was found in Trondheim from November to April during the period 1986-2015 [39]. Therefore, it is reasonable to believe that water loss due to evapotranspiration may have been neglected throughout the entire research period.
- Interception by the impermeable pavement has been neglected.
- There has been no overland flow due to a sufficiently large infiltration rate.

2.5 SWMM

The hybrid method [14] used for the snow process found in SWMM may perform in a different way compared to a full-scale energy balance method. Therefore, in this case a model of the same grey roof created by calibrated Low Impact Development (LID) module in EPA SWMM [29] has been utilized in order to compare it with the CM. The following

parameters will be calibrated in order to optimize the simulation result: 'Dividing Temperature Between Snow and Rain (T_{SR})', 'ATI Weight', 'Negative Melt Ratio (F_{MR})' in the snow melt and 'Min. Melt Coeff (C_{max}).', 'Max. Melt Coeff (C_{min}).', 'Base Temperature (T_{base})', 'Fraction Free Water Capacity (F_{fwc})' (see Appendix 4).

2.6 Calibration and assessing criteria

The calibration period has been determined to be the same as the previous research period. Additionally, there are two calibration criteria: the Nash-Sutcliffe Efficiency (NSE) and Relative Percentage Difference (RPD) of volume have been used for assessment:

$$\mathrm{NSE} = 1 - \frac{\sum_T (q_{obs} - q_{sim})^2}{\sum_T (q_{obs} - \overline{q_{obs}})^2}, \tag{15}$$

$$\mathrm{RPD} = \frac{\sum_T q_{sim} - \sum_T q_{obs}}{\sum_T q_{obs}}, \tag{16}$$

q_{obs} and q_{sim} are the observed and simulated runoff respectively during one-time sequence [l/min]; $\overline{q_{obs}}$ is the average of observed runoff.

NSE varies between minus infinity and 1; the closer it is to 1 means a better simulation result. A negative NSE indicates a simulation result worse than estimating by $\overline{q_{obs}}$.

A simulation result will also be assessed by the events used in section 2.3 to evaluate simulated peaks, as this result is anticipated to a certain degree. A special focus on the SD is required, as dynamic snow process dominates runoff from the grey roof. However, no physical measurement of SD was taken throughout the research period, resulting in the fact that using a camera to visually inspect the snow condition is the only way to compare it with simulated SD.

2.7 Limitations of the CM

The CM still cannot conceal its simplified process. First of all, intermediate measurements, for example the SD, ice content, temperature gradient in substrate are unknown, which hinders each sub-model's improvement. Secondly, the snow condition seen in the pictures shows that fusion occurred faster in the middle of the roof than at the edge of it. However, a uniform process, not area depletion, has been utilized in the snow pack model.

3 Result

3.1 Hydrological performance during winter

3.1.1 Analysis of the research period

The volume of cumulative runoff from the black roof was measured at 30.73m^3, and from the grey roof it was 28.15m^3. Both were greater than the total amount of precipitation measured during the research period: 26.44m^3, which might be explained by the fact that there was a thin ice layer present on the first research day. Figure 3.1 illustrates less cumulative runoff from the grey roof than the input from December 2017 to the end of March 2018. Moreover, the difference became greater from January to the middle of March. A sharp rise on the grey roof was observed from early April, a fact that had made the total runoff surpass that of the precipitation. However, the situation showed a significant difference with regard to the black roof. A high level of consistency occurred between the black roof's runoff and precipitation until the middle of February with the exception of three events. Furthermore, the final rise had contributed to a larger total runoff.

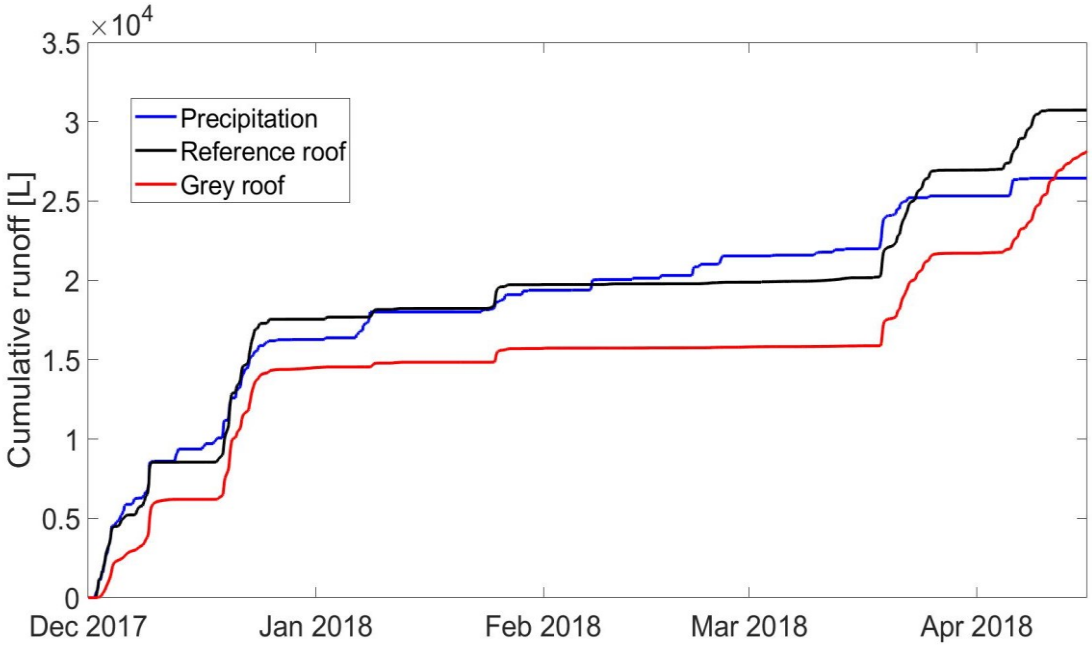

Figure 3.1. Cumulative runoffs from both black (black) and grey roofs (red) and cumulative hydrograph from the rain gauge (blue) during the whole research period.

3.1.2 Event-based analysis

Table 3.1 introduces the details regarding quantitative peaks and time delay as well as accumulated runoff from both the grey and black roofs after each event. An average of 34.62% (36.17% in median) in attenuation of peaks was obtained, where the largest reduction was 82.26% in early December and the smallest produced an increased peak (-20.44%) during a snowmelt and thawing event. The highest peaks from grey and black roofs both occurred in event 2, which also had the highest mean with respect to rainfall intensity.

Event	Peak				Accumulated		
	Runoff (l/min)		Reduction	Time delay	Runoff (L)		Reduction
	Grey	Black	(%)	(hh:mm)	Grey	Black	(%)
1	1.86	10.48	82.26	25:37	2241	4472	49.91
2	7.05	12.35	42.94	00:35	2695	2778	2.98
3	4.49	9.99	55.10	16:38	7857	8746	10.16
4	2.55	3.56	28.37	00:54	697	1207	42.21
5	4.07	4.50	9.45	00:10	4066	4715	13.78
6	1.26	1.79	29.40	-21:29	1633	1890	13.63
7	1.36	2.72	49.91	00:07	682	897	24.00
8	2.21	1.83	-20.44	73:05	5473	1206	-127.44

Table 3.1. Event-based analysis of hydrological performance for grey roof compared to black roof.

Regarding the delay in peak runoff, the average delay time was 12 hours and 10 minutes (45min in median) for all events. The largest postponement occurred in event 8, which was even 3 days later than that on the black roof. An increase in peak time was found after the snowmelt event (6). Noting that events 2, 4, 5, 7, showed a relatively poorer time delay (26.5min on average) compared to that during other events 1, 3, 6, 8 (23.65 hours on average). It was observed that the global peaks from both roofs during former 4 events came from the same sudden increase in precipitation intensity. Postponement of the latter four events was more unpredictable and could vary significantly. Moreover, a unique phenomenon was observed by analyzing synthetic temperatures and runoff from the grey roof in Figure 3.2 for events 1,4,5,7. The events' common features included a much later appearance and moderate increase of runoff and a transition of temperature in the substrate from below freezing temperatures to freezing temperature. Lab tests (Appendix 3) presented a similar situation, showing that HC tended to be larger in unfrozen substrate than that in frozen condition before runoff appeared from the outlet (breakthrough).

As concerns the accumulated runoff, an average reduction of 3.65% in total runoff from all events had been observed, see Figure 3.3a. A large amount of water storage (over 40%) happened in two events (1, 4), and a substantial release occurred in event 8 due to thawing. Up to 3200L of water stored as snow and ice during the winter was emptied in the early spring. There was no doubt that snowmelt coupled with thawing in event 8 had contributed to the second largest continuous runoff event for the entire research period.

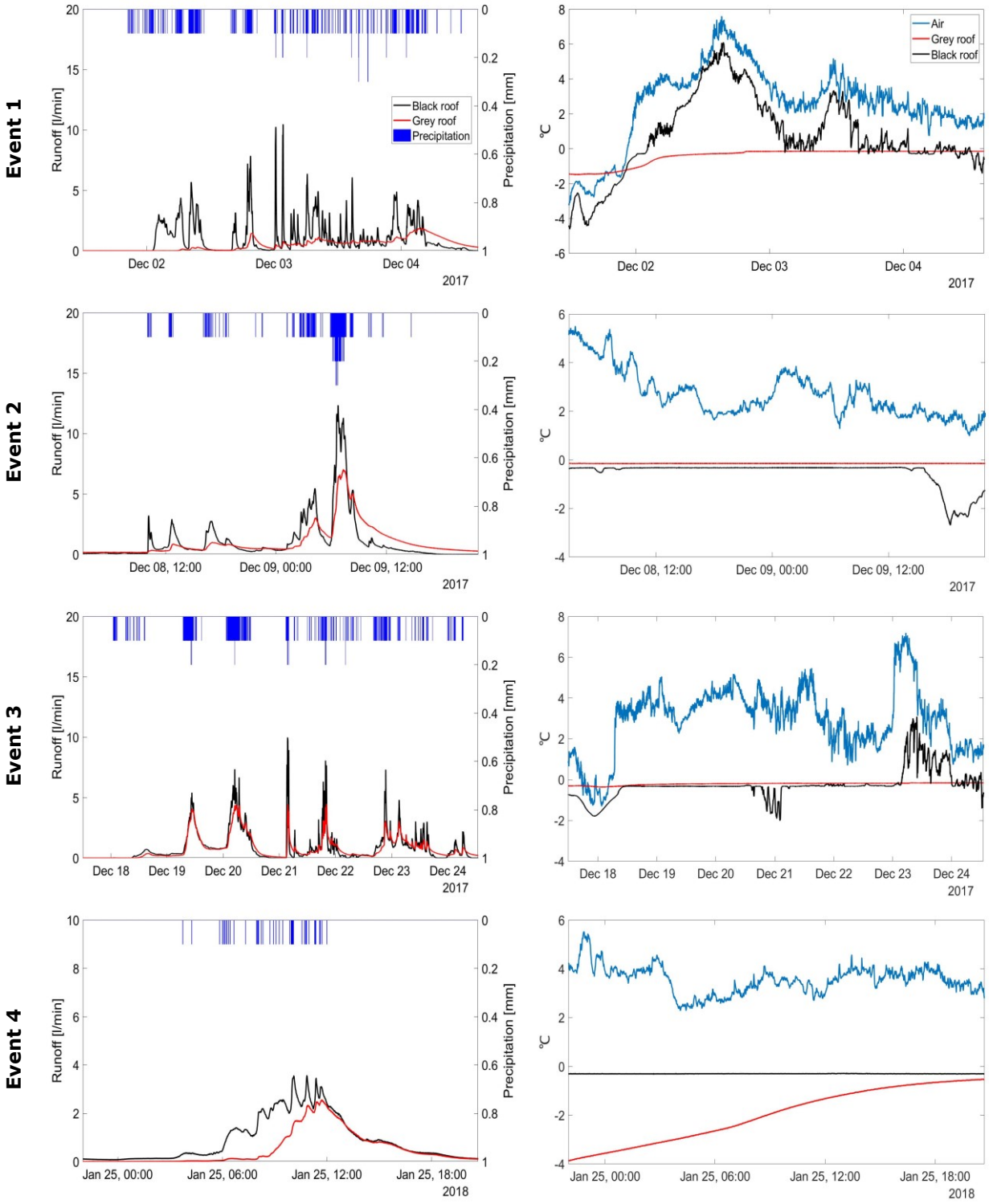

Figure 3.2. Cont.

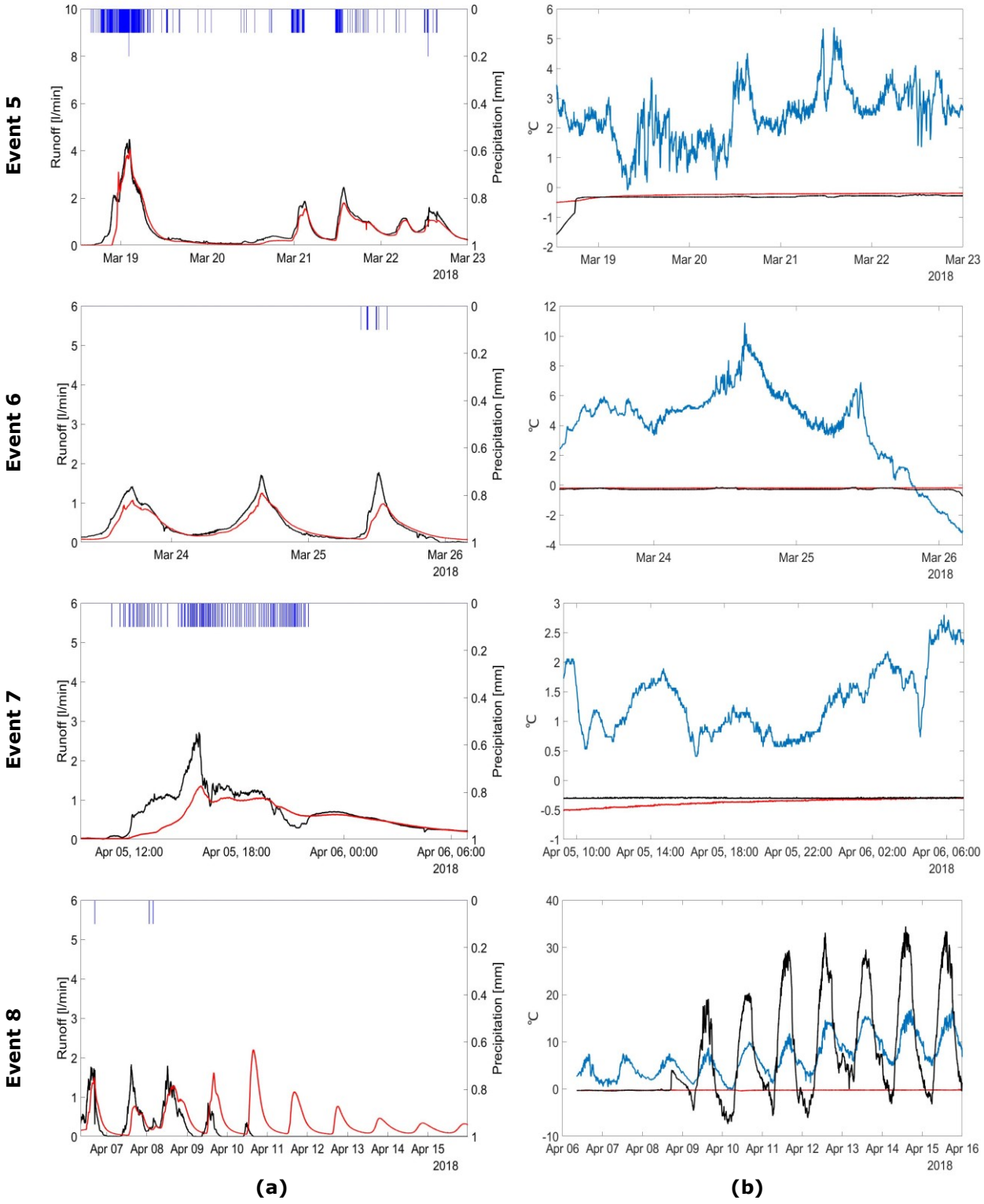

Figure 3.2. Event-based analysis: (a) Comparison of runoff from both black (black) and grey roofs (red); (b) Fluctuations of air temperature (blue) and temperatures on the surface of black roof (black) and at bottom of the grey roof (red).

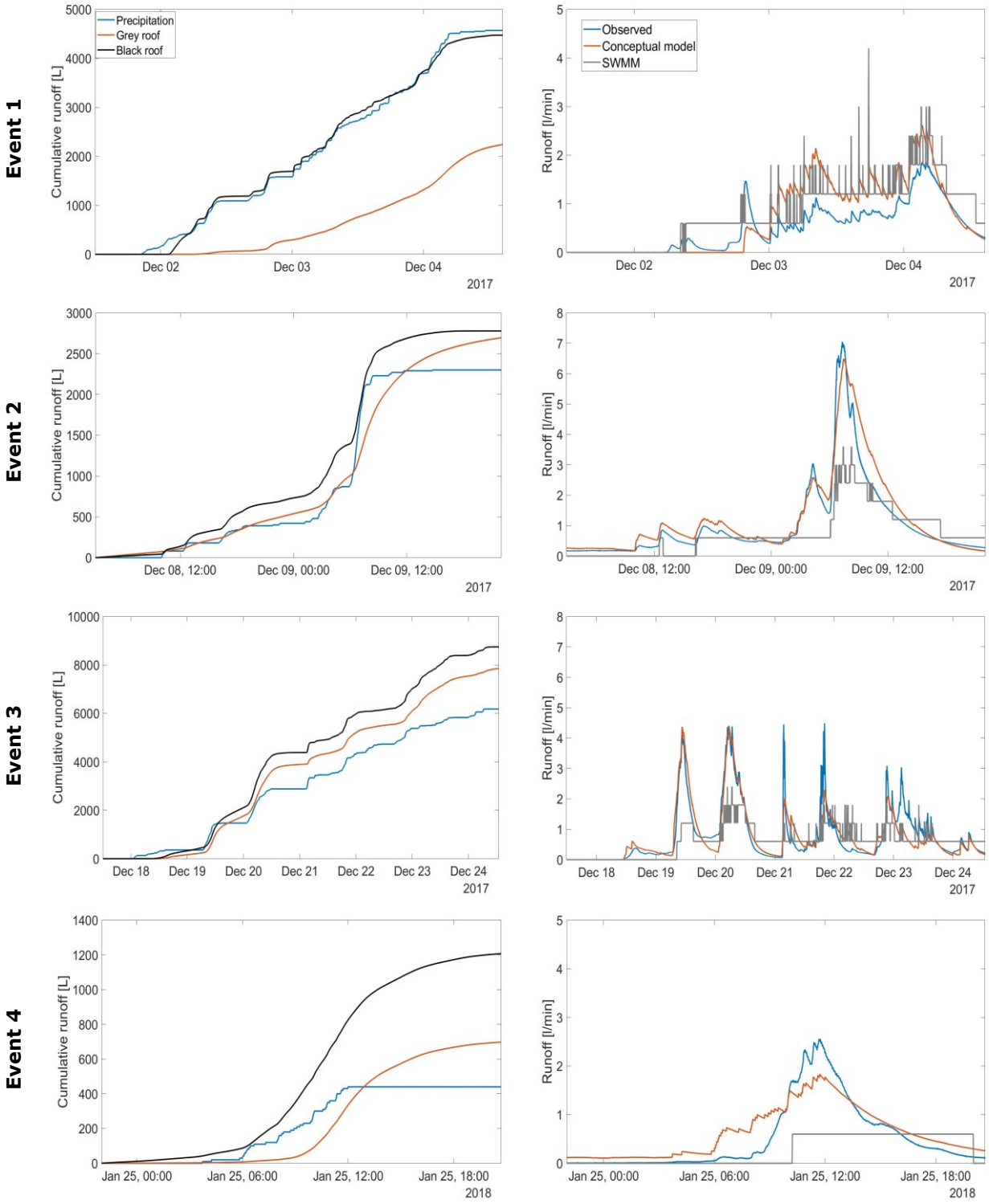

Figure 3.3. Cont.

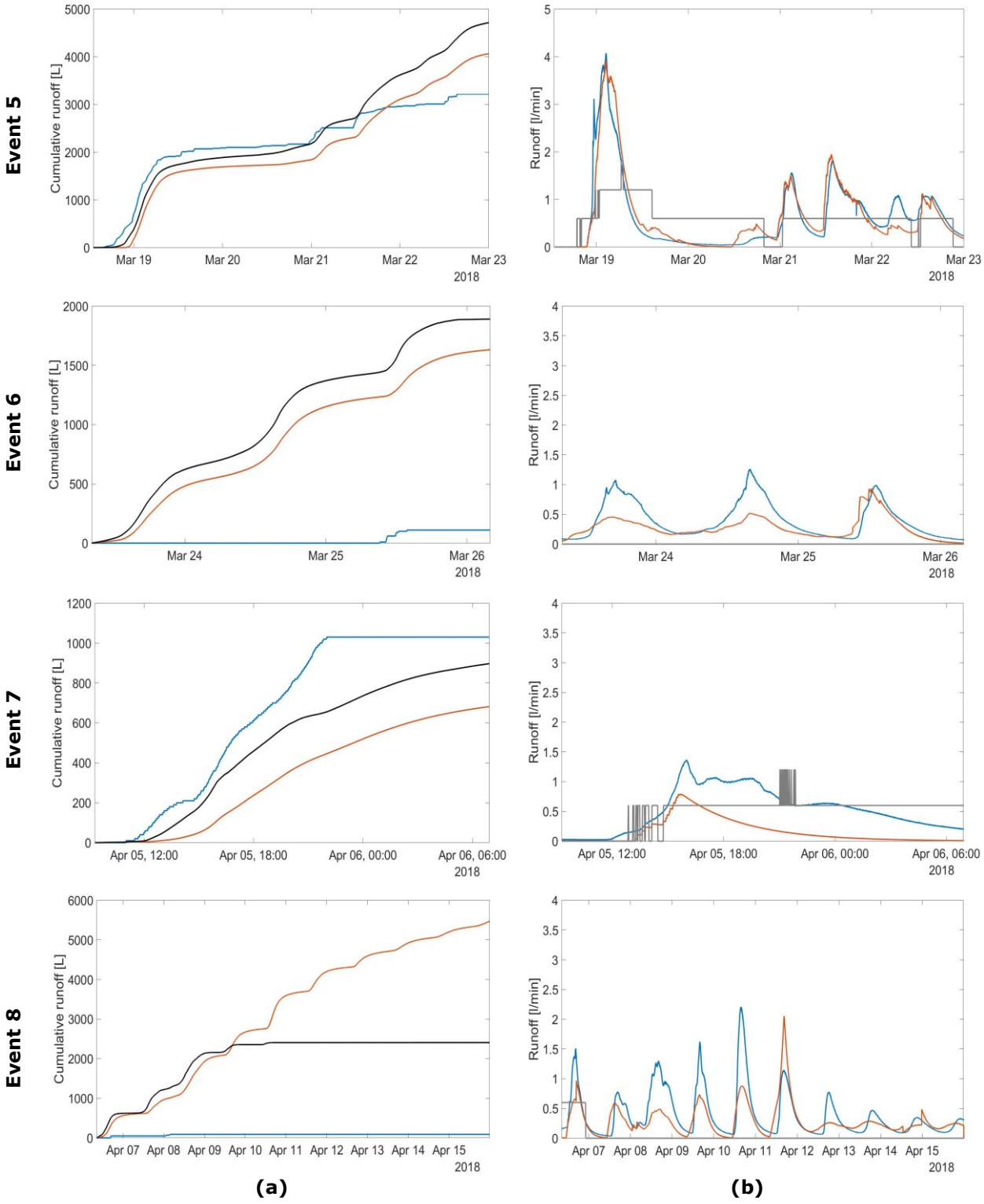

Figure 3.3. Event-based analysis: (a) Comparison of cumulative runoff from both black (black) and grey roofs (red) and cumulative hydrograph from the rain gauge (blue); (b) Observed (blue) and simulated runoff from both the CM (red) and SWMM (grey).

3.2 Simulation results of SWMM and the CM

The CM was calibrated by trying different values within a chosen interval of each parameter in Matlab. The parameter set obtaining the highest NSE was waiting for further improvement. This had to be done on the basis of events since different heat components dominated in different types of events. While, calibration for SWMM was proceeded manually and step by step. It was found that NSE changed slightly when adjusting values of the parameters.

The calibration results of both the SWMM and CM are shown in Appendix 2. β_1, β_2, β_3, β_4, β_5 are calibration parameters for the first to last terms in equation 2 with respect to the snow pack model. They were used for compensating for errors in each heat component caused by inaccurate measurements. Subsequently, β_6, β_7, β_8 were calibration parameters in equation 13a in the ice-water phase change model for compensating the simplified processes. The heat capacity of LECA (C_{leca}) was unfortunately not obtained from the manufactory. Thus, it was calibrated together with β_6. K_{uf} and K_f were HC-s in unfrozen and frozen substrate, 0.68 m/s and 1.5 m/s respectively after calibration. It was however summarized from lab tests that after the breakthrough, HC became similar in both frozen and unfrozen substrate with the same inflow.

3.2.1 The entire research period

The **CM** after the calibration achieved the NSE of 0.8403 and RPD of -3% (Table 3.2). The observed runoff and that simulated by CM were almost identical, as shown in Figure 3.4. On the other hand, the analysis from the cumulative runoff in Figure 3.5 illustrates an overestimation of runoff in the early period; it also affects the parallel stage, which shows improved simulations until an underestimation occurs in April. The unmatched accumulated simulated runoff was the reflection of event-based biases which would be mentioned in the following sub-section.

Model	NSE	RPD
CM	0.8403	-3.1%
SWMM	0.3862	-7.1%

Table 3.2. Obtained NSE and RPD by both CM and SWMM after calibration during the entire research period.

However, **SWMM** poorly simulated runoff for the entire period. And the result was reflected by a low NSE of 0.3862 and relatively good RPD of -7.1%. In addition, the poor accuracy (0.01 l/s precision equivalent to 0.6 l/min) made it difficult to follow precisely any minor changes in runoff, for example local peaks and mitigations. There were in total 8 visible runoff events simulated by SWMM that in fact did not show up in reality. In addition, it showed a growing overestimation by SWMM before April, followed by mild runoff events.

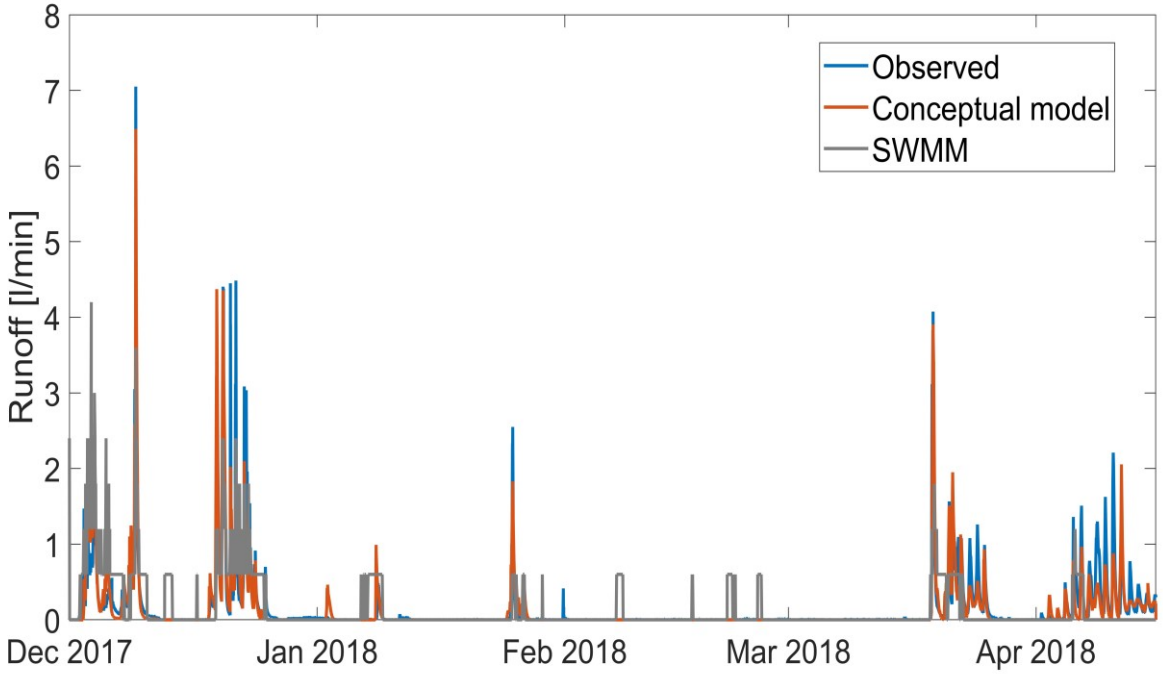

Figure 3.4. Simulated runoff by both SWMM (grey) and CM (red) compared to the observed runoff (blue) from the grey roof.

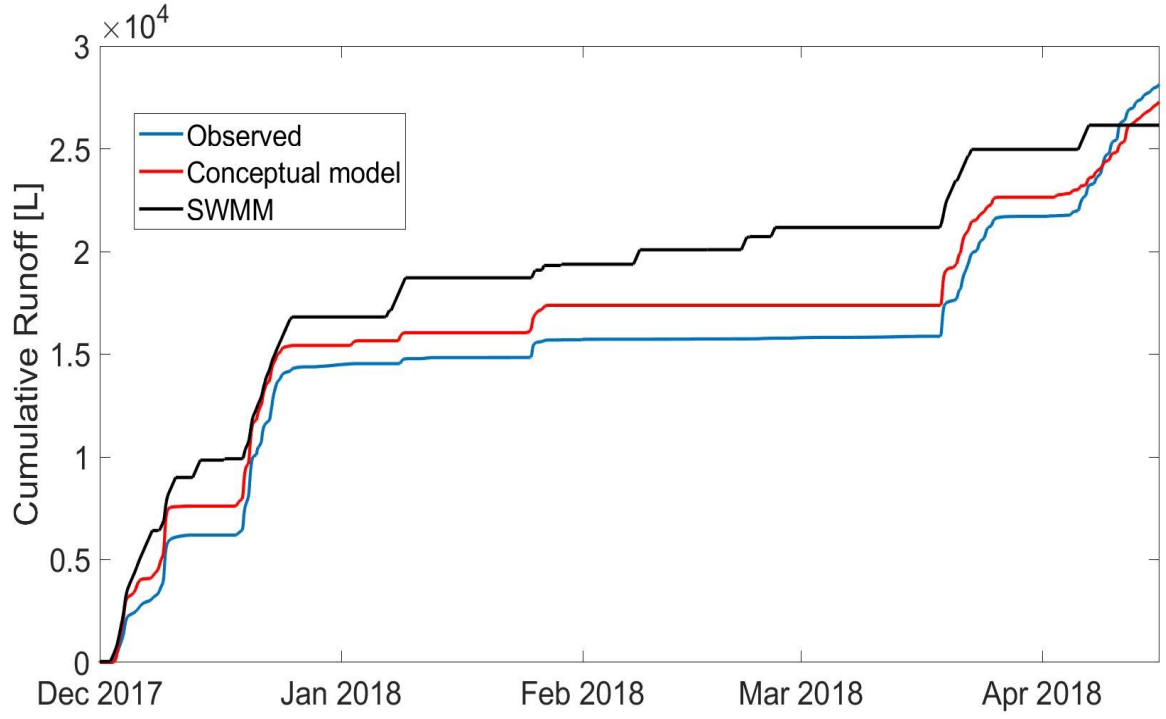

Figure 3.5. Simulated cumulative runoff by both SWMM (black) and CM (red) compared to the observed cumulative runoff (blue) from the grey roof.

3.2.2 Event-based simulation

The eight events were also good indicators for assessing simulation results for both models. The NSEs by both CM and SWMM are summarized for each event in Table 3.3. Four larger events (2, 3, 4, 5) with NSE over 0.8 were simulated by the CM, while they produced relatively poor results for shorter and smaller events (1, 6, 7, 8). Figure 3.3b also shows that in well-performed events, runoff fluctuations were highly similar to the real cases except in certain biases of three local peaks in event 3 and the peak in event 4. However, in these events SWMM successfully simulated only in event 2, as it had an NSE above 0.5, yet at the same time poor peak simulations. Both models presented unsatisfied performance and overestimation in event 1. The worst simulated events by the CM and SWMM were 7 and 6 respectively. A significant underestimation in event 7 revealed poor performance by the CM for single and small runoff events. SWMM failed to present runoff in both snowmelt events. In event 8 the CM was able to mimic the fluctuation, showing a successful application of ice-water phase change model. Quantitative simulation of thawing was, however, not very satisfying.

NSE	CM	SWMM
Event 1	0.1586	0.1727
Event 2	0.9057	0.5504
Event 3	0.8415	0.4287
Event 4	0.8005	0.2081
Event 5	0.8848	0.2211
Event 6	0.4049	-1.7388
Event 7	-0.4597	0.3385
Event 8	0.4617	-0.8164

Table 3.3. Event-based NSE-s by the CM and SWMM.

3.2.3 Snow depth

As shown in Figure 3.6, the chosen 12 time points (TP) traced the variation of snow depth (SD). A first glance showed that simulated SD by CM was very consistent with reality, whereas a certain number of disagreements by SWMM were found in early and late December and the close of the research period. SD by CM at TP 1 and 2 showed the opposite result, as snow appeared more on the grey roof at TP 2 than it did at TP 1. A 5mm difference of SD by CM between TP 8 and 9 might not be easily observed in the pictures. But at TP 10 a fully snow-covered grey roof made it unique from other TPs. The final appearance of snow by CM was obtained at 16:30 on 11 April and observed in reality from the picture at noon on 12 April. SD by SWMM showed the same result as CM between TP 2 and 3. Starting in January, a long-term underestimation might be observed, and heavy amounts of simulated snow by SWMM remained on the grey roof until the last minute.

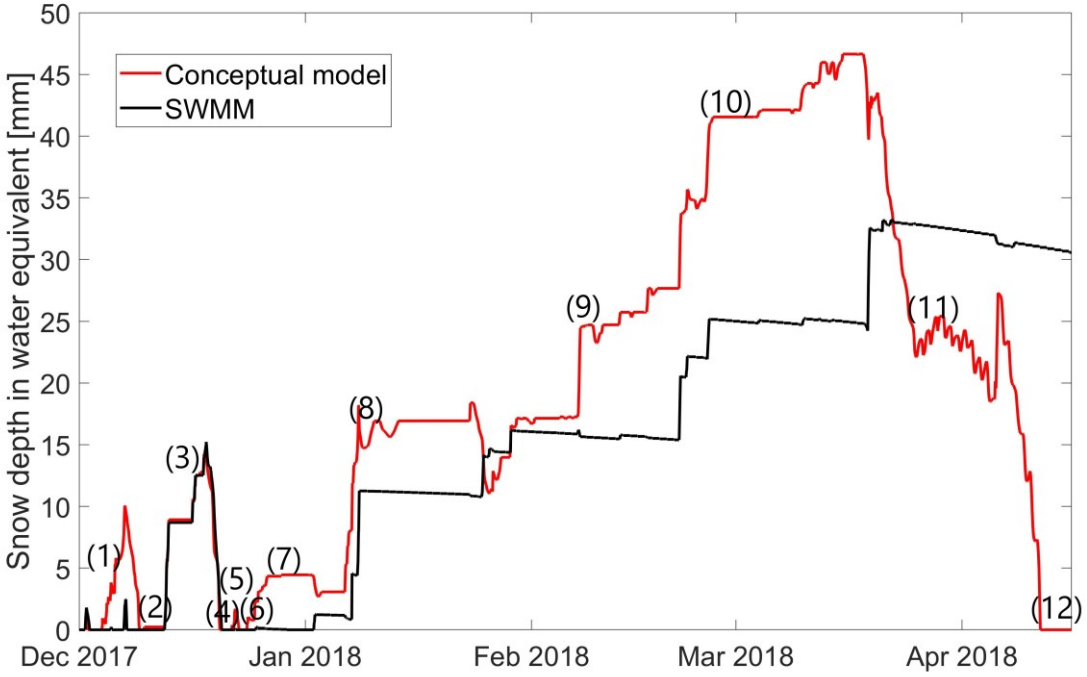

(a)

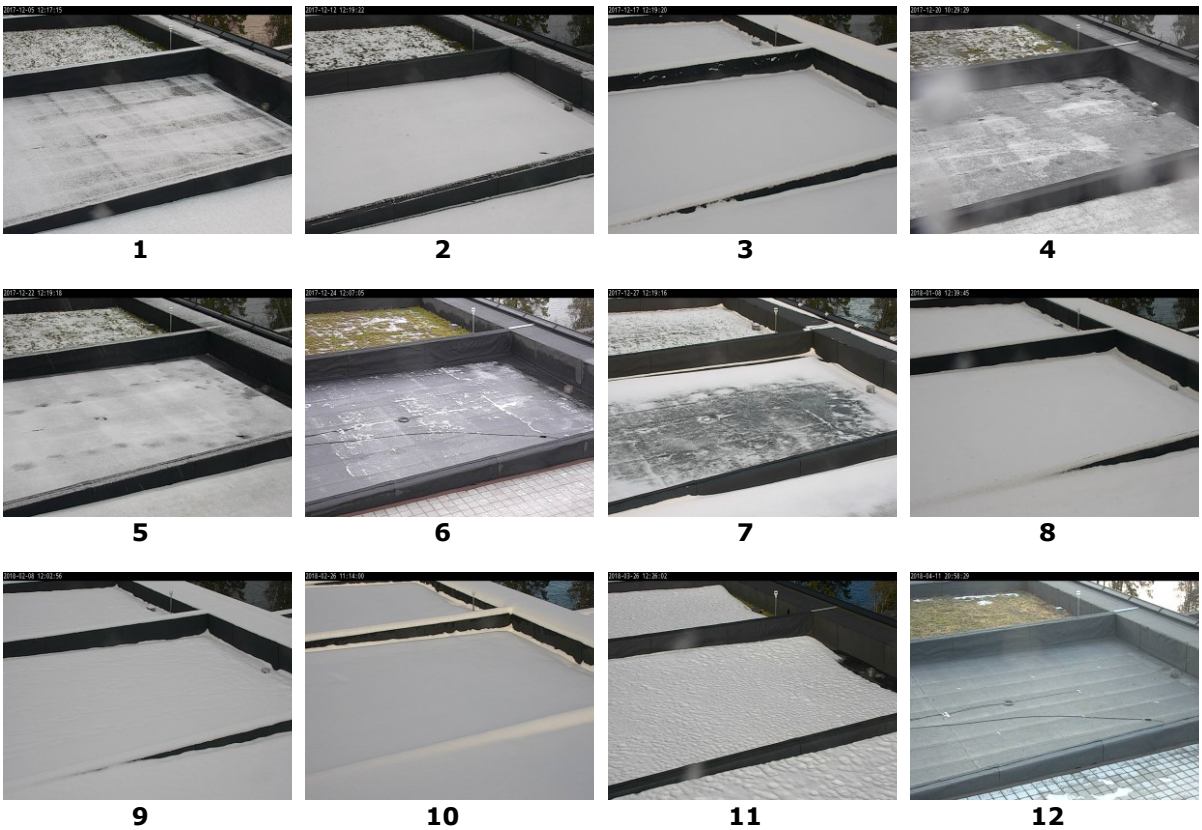

(b)

Figure 3.6. An evaluation of simulated SD by comparing to the snow condition recorded by camera at 12 chosen time-points: (a) Simulated SD by both CM (red) and SWMM (black); (b) Snow condition on three different roofs, in which the closest is the grey roof.

4 Discussion

Recalling the main objective of this study and the three research questions proposed in the introduction, a discussion will take place regarding the obtained results. The grey roof's retention and detention capacities are indicated by event-based analysis, showing prominent performance during the winter months. In addition, the CM obtained a good runoff simulation compared to the SWMM model. However, the detailed process described by CM may not fit well with the real case from the available data source. Limitations and applications of the CM are also specifically discussed in this section.

4.1 Hydrological performance

Attenuation of peak flow by the same grey roof has been observed to range from 80% to 97% in warmer seasons compared to 9.45% to 82.26% during winter, as well as a more rapid occurrence of the peak in general [3]. This attenuation may be attributed to several reasons: (1) Intensity of precipitation. It has been observed from both studies that rapid precipitation events result in larger reductions of peak runoff by the grey roof but shorter peak time delay; (2) Initial negative temperature. Initial frost may obstruct the flow path until water melts some ice and find its way out. This has also been identified by lab tests, as shown in Appendix 3, and supported by rain gardens' study in Trondheim [40] and soil research in Alaska [41]. Because of the snowmelt and thawing, larger peak runoff and advanced peak time can occur during winter. Fortunately, from a quantitative point of view, this does not pose a threat to the drainage system, although longer-duration runoff is to be expected.

Another issue regarding predicting peak time delay is also of great interest, as initial water content, precipitation pattern and duration may all influence the final result. Brief precipitation comprised of a single downpour makes peak time from both black and grey roofs similar, and in this case a quick peak response by the grey roof may be confirmed. On the other hand, long-lasting and more uniform precipitation as well as snowmelt make the situation complex and extremely difficult to predict. Since both parameters (peak reduction and time delay) influence the practical implications for drainage systems [3], more effective methods for analyzing peak time delay need to be developed.

4.2 Conceptual model

Calibrated β values result in offset for f.ex. solar radiation between simulated results and reality, whereas unadjusted estimations of each component seem to hardly simulate each heat source [19]. Simulated heat components may unfortunately not be identified in this study. The relatively well simulated snow condition is on the one hand a positive reflection of an appropriate simulation approach for the roofing environment compared to the partial energy-balance budget used in SWMM. On the other hand, there is compensation between each component because of β-s. Hence, it is essential to obtain verification during a second winter period.

It is actually a dilemma that initial water and ice contents have been estimated by observed permittivity and temperature, since these will affect the trends of simulated ice and water contents. Stable, high simulated water content is in fact in contradiction with extreme low temperatures in the substrate in January and February [26]. This can be explained by

assuming unchanged FC (see 2.4.4) throughout the entire winter. However, another model [25] showed that runoff could still occur through low and high domains without reaching FC, so the application of FC in frozen substrate shall be reconsidered. As water content affects ice-water phase change in return, it is reasonable to doubt that simulated ice content deviates from reality.

It is always interesting to discuss how HC changes with the presence of frost in different substrates [12,26]. Both water content at the moment of freezing and aggregate types are influential factors in this process. Concepts of granular frost and porous frost as well as preferential flow paths [42] may explain an enlarged calibrated HC. Unfortunately, the lab tests did not support the hypothesis. It showed that HC in frozen substrate was equal or smaller than that in unfrozen condition. The result of lab tests was also observed by other types of frozen soils [43,44].

4.3 Limitations and applications

As mentioned above, the lack of intermediate data makes it difficult to find out drawbacks of each sub-model and discard β-s. This leads to site limitation of the CM, as β-s may vary from site to site. Moreover, without having a second winter period to test validity at the same place, it is also conceivable that the CM is time-specific. If the snow equivalent water depth would have been obtained, then it would have been realistic to optimize the snow pack sub-model. More accurate drainage flow from snowmelt could be of great help in improving the ice-water phase change and grey roof sub-models. It should also be noted that ground heat neglected in the CM may play an important role in this process since the melting rate actually differs quite a bit between the green, black and grey roofs observed from the camera (Figure 3.6b). At last, freezing and thawing cycles will reduce HC of Leca whereas the minimum HC (0.3 cm/s) is restricted by German FLL recommendations [43]. However, the CM was not able to precisely assess HC of the Leca during winter, and would not provide reliable theoretical support for maintenance of the grey roof, for example replacement of Leca.

Despite its limitations, the CM still shows potential. First of all, it provides a simplified method for interpreting and predicting processes for roof environments from snowfall to runoff. The positive simulation results for large runoff events supports relatively reliable predictions for extreme rain on snow and snowmelt events. Thus, it is believable that the prediction will help with decisions for site selection for grey roof installation and drainage system design. Hence, risks of stormwater during winter and early spring can be mitigated considerably. Secondly, it is possible for the CM to apply on other grey roofs with different configurations or on green roofs. This can be done by modifying the substrate's thermal and mechanical parameters for other grey roofs or applying green roof model for green roofs.

5 Conclusion

This study may be regarded as a continuation of the same grey (LECA) roof studied by Hamouz [3,29] during winter. The evaluation has been concerned with retention and detention capacities through both long-term and event-based analysis. A new conceptual model consisting of three sub-models has also been applied in order to simulate runoff from the grey roof during the winter of 2017-2018.

The eight largest runoff events demonstrate a good detention capacity (34.62% average attenuation of peak flow ranging from -20.44% to 82.26% and average time delay 12 hours 10 minutes ranging from -21 h 29 min to 73 h 05 min) by the grey roof. The reduction of peak flow is weak compared with warm seasons while postponement is strengthened. In addition, snowmelt events cause unstable factors, as both greater peak runoff and advanced peak time happened when the snow melted. Generally, the grey roof having 1.5-2.5mm LECA can still play a role in controlling and reducing risks of rain on snow and spring melt events.

It has also been identified by applying the CM and SWMM that the energy balance method is more suitable for the snow pack sub-model for roof environments. But without the deeper exploration of each heat component and real data for comparison, simulated results will most likely deviate from reality because of the intrusive correcting factors. On the other hand, the attempt to analyze water flow in frozen substrates using ice-water phase change and green roof sub-models achieved good runoff simulation results. Similarly, proposed calibrated parameters such as FC and HC, as well as simulated ice- and water contents, seemed to be limited by mathematical process instead of mimicking the real case.

More work is encouraged to improve the CM and make estimations on water and ice contents more accurate. It is also worth expecting that the CM can be applied on the same grey roof for more winter periods or other grey/green roofs located in different places. The simplified process of modelling is highly recommended for the analysis of hydrological principles of grey/green roofs. Concrete knowledge will most likely promote the development of these special roofs and improve the severe situation caused by stormwater in urban area.

Reference

1. Stovin, V.; Vesuviano, G.; Kasmin, H. The hydrological performance of a green roof test bed under UK climatic conditions. *Journal of Hydrology* **2012**, *414*, 148-161.
2. Johannessen, B.G.; Muthanna, T.M.; Braskerud, B. Detention and retention behavior of four extensive green roofs in three nordic climate zones. *Journal of Water* **2018**, *10*, 671.
3. Hamouz, V.; Lohne, J.; Wood, J.; Muthanna, T.M. Hydrological performance of LECA-based roofs in cold climates. *Journal of Water* **2018**, *10*, 263.
4. Kunkel, K.E.; Robinson, D.A.; Champion, S.; Yin, X.; Estilow, T.; Frankson, R.M. Trends and extremes in northern hemisphere snow characteristics. *Current Climate Change Reports* **2016**, *2*, 65-73.
5. Wang, G.; Hu, H.; Li, T. The influence of freeze–thaw cycles of active soil layer on surface runoff in a permafrost watershed. *Journal of Hydrology* **2009**, *375*, 438-449.
6. Thorolfsson, S.T.; Brandt, J. The influence of snowmelt on urban runoff in Norway. In Proceedings of Proc. 7th Int. Conf. On Urban Storm Drainage.
7. Semadeni-Davies, A.; Bengtsson, L. Snowmelt sensitivity to radiation in the urban environment. *Hydrological Sciences Journal* **1998**, *43*, 67-89.
8. Bengtsson, L.; Westerström, G. Urban snowmelt and runoff in northern Sweden. *Hydrological sciences journal* **1992**, *37*, 263-275.
9. Cherkauer, K.A.; Lettenmaier, D.P. Hydrologic effects of frozen soils in the upper Mississippi River basin. *Journal of Geophysical Research: Atmospheres* **1999**, *104*, 19599-19610.
10. Xiuqing, Z.; Flerchinger, G.N. Infiltration into freezing and thawing soils under differing field treatments. *Journal of Irrigation and Drainage Engineering* **2001**, *127*, 176-182.
11. Niu, G.-Y.; Yang, Z.-L. Effects of frozen soil on snowmelt runoff and soil water storage at a continental scale. *Journal of Hydrometeorology* **2006**, *7*, 937-952.
12. Paus, K.H.; Muthanna, T.M.; Braskerud, B.C. The hydrological performance of bioretention cells in regions with cold climates: seasonal variation and implications for design. *Journal of Hydrological Research* **2016**, *47*, 291-304.
13. Semádeni-Davies, A.F. Representation of snow in urban drainage models. *Journal of Hydrologic Engineering* **2000**, *5*, 363-370.
14. Moghadas, S.; Gustafsson, A.-M.; Muthanna, T.M.; Marsalek, J.; Viklander, M. Review of models and procedures for modelling urban snowmelt. *Journal of Urban Water* **2016**, *13*, 396-411.
15. Valeo, C.; Ho, C.L.I. Modelling urban snowmelt runoff. *Journal of Hydrology* **2004**, *299*, 237-251.
16. Sundin, E.; Andreasson, P.; Viklander, M. An energy budget approach to urban snow deposit melt. *Journal of Hydrology Research* **1999**, *30*, 39-56.
17. Matheussen, B.V. Effects of anthropogenic activities on snow distribution, and melt in an urban environment. Doctoral thesis, Norwegian University of Science and Technology, 2004.

18. Martinec, J. Snowmelt-runoff model for stream flow forecasts. *Journal of Hydrology Research* **1975**, *6*, 145-154.

19. Walter, M.T.; Brooks, E.S.; McCool, D.K.; King, L.G.; Molnau, M.; Boll, J. Process-based snowmelt modeling: does it require more input data than temperature-index modeling? *Journal of Hydrology* **2005**, *300*, 65-75.

20. Anderson, E.A. *A point energy and mass balance model of a snow cover*; Department of commerce: 1976.

21. Jayasooriya, V.M.; Ng, A.W.M. Tools for modeling of stormwater management and economics of green infrastructure practices: a review. *Journal of Water, Air, Soil pollution* **2014**, *225*, 2055.

22. Locatelli, L.; Mark, O.; Mikkelsen, P.S.; Arnbjerg-Nielsen, K.; Jensen, M.B.; Binning, P.J. Modelling of green roof hydrological performance for urban drainage applications. *Journal of Hydrology* **2014**, *519*, 3237-3248.

23. Kasmin, H.; Stovin, V.R.; Hathway, E.A. Towards a generic rainfall-runoff model for green roofs. *Journal of Water Science and Technology* **2010**, *62*, 898-905.

24. Stovin, V.; Poë, S.; Berretta, C. A modelling study of long term green roof retention performance. *Journal of Environmental Management* **2013**, *131*, 206-215.

25. Manfred, S.; Per-Erik, J.; Lundin, L.-C. Preferential water flow in a frozen soil — a two-domain model approach. *Journal of Hydrological Processes* **1996**, *10*, 1305-1316.

26. Lundin, L.-C. Hydraulic properties in an operational model of frozen soil. *Journal of Hydrology* **1990**, *118*, 289-310.

27. Cipolla, S.S.; Maglionico, M.; Stojkov, I. A long-term hydrological modelling of an extensive green roof by means of SWMM. *Ecological engineering* **2016**, *95*, 876-887.

28. Johannessen, B.G.; Hamouz, V.; Gragne, A.S.; Muthanna, T.M. The transferability of SWMM model parameters between green roofs with similar build-up. *Journal of Hydrology* **2019**, *569*, 816-828.

29. Hamouz, V.; Muthanna, T.M. Modelling of Green and Grey Roofs in Cold Climates Using EPA's Storm Water Management Model. Cham; pp. 385-391.

30. Klima2050. Klima2050. Availabe online: http://www.klima2050.no/ (accessed on 22.04.2019).

31. yr. Været som var Trondheim (Voll) målestasjon, Trondheim (Trøndelag). Availabe online: https://www.yr.no/sted/Norge/Tr%C3%B8ndelag/Trondheim/Trondheim_(Voll)_m%C3%A5lestasjon/statistikk.html (accessed on 19.04.2019).

32. Thorolfsson, S.T.; Matheussen, B.V.; Frisvold, H.; Nilsen, O.; Kristiansen, V.; Pedersen-Oeverleir, A. Urban hydrological data collection in cold climate. Experiences at Risvollan, Trondheim, Norway. In Proceedings of Proceedings of the 1st International conference on urban drainage and highway runoff in cold climates, IWA, IAHR, Luleaa University of Technology; pp. 303-313.

33. Peacock, E.E. *Monitoring the in situ archaeological deposits at Schultzgt. 3-7, Trondheim, Norway (1996-2001)*; 2002.

34. NRK. Motorsyklist alvorlig skadd i trafikkulykke. Availabe online: https://www.nrk.no/trondelag/motorsyklist-alvorlig-skadd-i-trafikkulykke-i-trondheim-1.13090230 (accessed on 07.06.2019).

35. Chýlek, P.; Ramaswamy, V.; Srivastava, V. Albedo of soot-contaminated snow. *Journal of Geophysical Research: Oceans* **1983**, *88*, 10837-10843.

36. Snyder, W.C.; Wan, Z.; Zhang, Y.; Feng, Y.-Z. Classification-based emissivity for land surface temperature measurement from space. *International Journal of Remote Sensing* **1998**, *19*, 2753-2774.

37. Laboratories, S.N. Extraterrestial radiation. Availabe online: https://pvpmc.sandia.gov/modeling-steps/1-weather-design-inputs/irradiance-and-insolation-2/extraterrestrial-radiation/ (accessed on 20.04.2019).

38. Buck, A.L. New equations for computing vapor pressure and enhancement factor. *Journal of Applied Meteorology* **1981**, *20*, 1527-1532.

39. Johannessen, B.G.; Hanslin, H.M.; Muthanna, T.M. Green roof performance potential in cold and wet regions. *Journal of Ecological Engineering* **2017**, *106*, 436-447.

40. Muthanna, T.M.; Viklander, M.; Thorolfsson, S.T. Seasonal climatic effects on the hydrology of a rain garden. *Journal of Hydrological Processes: An International Journal* **2008**, *22*, 1640-1649.

41. Kane, D.L.; Stein, J. Water movement into seasonally frozen soils. *Water Resources Research* **1983**, *19*, 1547-1557.

42. LeFevre, N.J.; Davidson, J.D.; Oberts, G.L. Bioretention of simulated snowmelt: Cold climate performance and design criteria. In Proceedings of Proceedings of the 14th Conference on Cold Regions Engineering; pp. 145-154.

43. Gwóźdź, K.; Hewełke, E.A.; Sas, W.; Żakowicz, S.; Baryła, A. Influence of cyclic freezing and thawing on the hydraulic conductivity of selected aggregates used in the construction of green roofs. *Journal of Ecological Engineering* **2016**, *17*, 50--56.

44. McCauley, C.A.; White, D.M.; Lilly, M.R.; Nyman, D.M. A comparison of hydraulic conductivities, permeabilities and infiltration rates in frozen and unfrozen soils. *Cold Regions Science and Technology* **2002**, *34*, 117-125.

Appendix

Appendix 1: Detailed derivation

Appendix 2: Calibrated parameters

Appendix 3: Lab tests

Appendix 4: SWMM interface

Appendix 5: Matlab code

Appendix 1 Detailed derivation

Derivation of the one-dimensional energy conservation equation for the ice-water phase change model in section 2.4.3:

The energy conservation equation consists of 4 terms: the first and second terms on the left side describe respectively sensible and latent heat; The first term on the right side is the divergence of the heat flow, and the second term refers to the convective heat from infiltrated water.

$$\frac{\partial(\mathrm{CT})}{\partial \mathrm{t}} - \mathrm{L_i}\rho_\mathrm{i}\frac{\partial \theta_\mathrm{i}}{\partial \mathrm{t}} = \frac{\partial}{\partial \mathrm{z}}\left(\mathrm{k_h}\frac{\partial \mathrm{T}}{\partial \mathrm{z}}\right) - \mathrm{C_w}\frac{\partial(\mathrm{Tq_w})}{\partial \mathrm{z}},$$

$$\frac{\partial \mathrm{C}}{\partial \mathrm{t}}\mathrm{T} + \frac{\partial \mathrm{T}}{\partial \mathrm{t}}\mathrm{C} - \mathrm{L_i}\rho_\mathrm{i}\frac{\partial \theta_\mathrm{i}}{\partial \mathrm{t}} = \frac{\partial \mathrm{k_h}}{\partial \mathrm{z}}\left(\frac{\partial \mathrm{T}}{\partial \mathrm{z}}\right) + \mathrm{k_h}\frac{\partial^2 \mathrm{T}}{\partial \mathrm{z}^2} - \mathrm{C_w}\left(\frac{\partial \mathrm{T}}{\partial \mathrm{z}}\mathrm{q_w} + \mathrm{T}\frac{\partial \mathrm{q_w}}{\partial \mathrm{z}}\right),$$

It is assumed that the heat capacity of LECA remains constant at different temperatures and the temperature gradient in the substrate is 0℃/m. Thus, the first term on the left side, and the first, second, and third terms on the right side become all 0-s. The final form then becomes:

$$\mathrm{L_i}\rho_\mathrm{i}\frac{\partial \theta_\mathrm{i}}{\partial \mathrm{t}} = \frac{\partial \mathrm{T}}{\partial \mathrm{t}}\mathrm{C} + \mathrm{C_w}\mathrm{T}\frac{\partial \mathrm{q_w}}{\partial \mathrm{z}},$$

The term on the left side denotes the change of ice content. While the two terms on the right side are heat released or absorbed by LECA due to temperature changes and convective heat by infiltrated water respectively.

Appendix 2 Calibrated parameters

Calibrated parameters for both CM and SWMM:

Sub-model	Parameters	Calibrated value
Snow pack	β_1	6
	β_2	1
	β_3	0.0001085
	β_4	2.8
	β_5	9
	γ	0.9
	Fr	0.15
Ice-water heat change	$C_{leca}\beta_6$	600
	β_7	0.2
	β_8	4.5
Grey roof	K_{uf}	0.68
	K_f	1.5

Table A2.1. Calibrated parameters in different sub-models in CM.

Sub-module	Parameters	Calibrated value
Snow pack	C_{max}	0.5
	C_{min}	1.2
	T_{base}	2
	F_{fwc}	1
Snow melt	T_{SR}	0.8
	ATI	1
	F_{MR}	0.6

Table A2.2. Calibrated parameters in the snowpack and snow-melt modules in SWMM

Appendix 3 Lab tests

Laboratory tests to verify HC in both frozen and unfrozen Leca:

The lab column test was implemented in order to evaluate HC in 1.5-2.5mm Leca in different aggregate conditions (frozen and unfrozen). It was carried out by filling up a glass column with saturated Leca with one side connecting to the tap and outlet to the other side, see Figure A3.1. The first step was to let the Leca drain for 2 hours before each test in order to reach field capacity (FC). Once the tap was open for inflow, video recording of weight of the total outflow started until outflow became little and discontinuous. Meanwhile, the valve controlling the inflow was shut down after outflow became stable. This had been fulfilled five times with various inflow from 3.3 to 8.0 l/min for unfrozen substrate.

Figure A3.1. Lab column test for estimations of hydraulic conductivity in both unfrozen and frozen aggregate conditions.

The second step was to put the whole column (Leca in FC) in refrigerator under -10℃ for 24 hours to ensure completely frozen aggregate. Thereafter, the same test was implemented for the frozen column under room temperature with inflow temperature of around 8℃. This was repeated for three times. A complete overview of the lab test is illustrated in Table A3.1. The inflow and time of valve-off for frozen tests (6,7,8) were controlled to be identical as those for three of the unfrozen tests (3,4,5) in order to control variables.

The last step was to read outflow from the video for every 5 seconds from all 8 tests and plotted them into a figure as shown in Figure A3.2. Longer breakthrough time (time from start of flow to observed runoff at outlet) in general was observed for frozen substrate than that for unfrozen with the same inflow. This has identified a smaller HC for frozen substrate in the case of same inflow before breakthrough. However, after water started to run off, increasing rate of flow were similar and declining trends overlapped for the same inflow in frozen and unfrozen conditions. The observation implied equivalent hydraulic conductivities for both conditions after the breakthrough.

Substrate condition	Number of tests	Inflow	Valve-off	Time to breakthrough
		[l/min]	[s]	[s]
Unfrozen	1	7.122	115	30
	2	5.314	170	45
	3	3.336	350	55
	4	4.710	330	45
	5	8.024	140	35
Frozen	6	3.436	350	75
	7	4.638	330	75
	8	7.820	140	50

Table A3.1. An overview of lab processes and observations for 8 total flow tests.

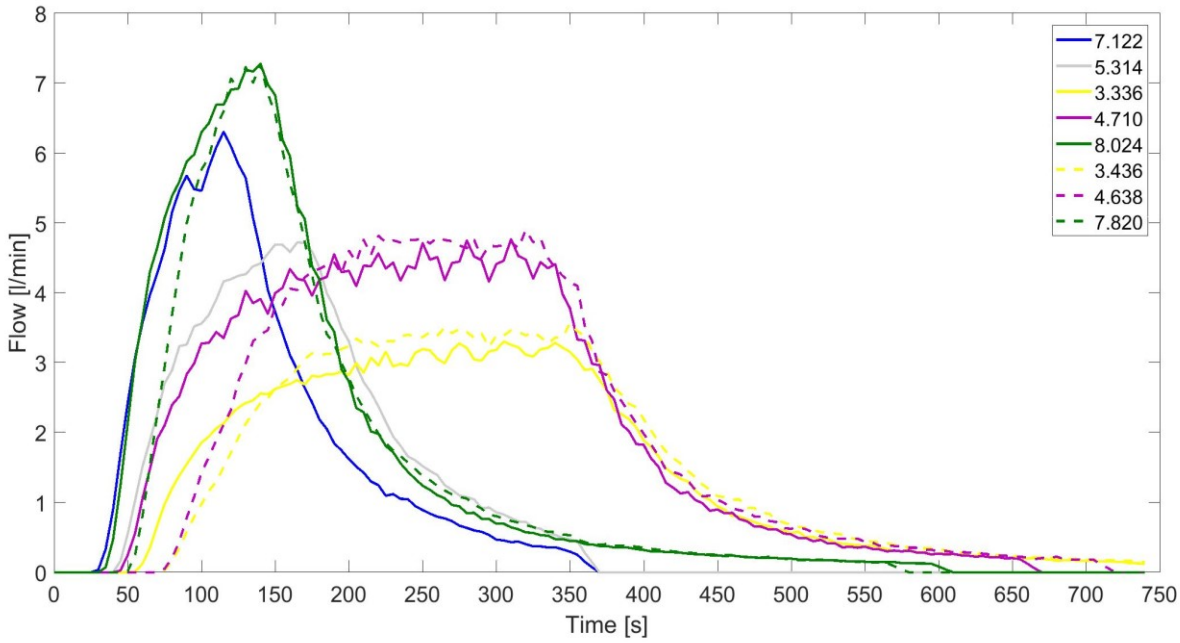

Figure A3.2. The legend refers to the inflow in [l/min] from all 8 lab tests; Solid lines are unfrozen aggregate, and dash lines indicate frozen aggregate; Identical inflows in both conditions are plotted in same color.

Appendix 4 SWMM interface

SWMM interface to simulate runoff from the grey roof:

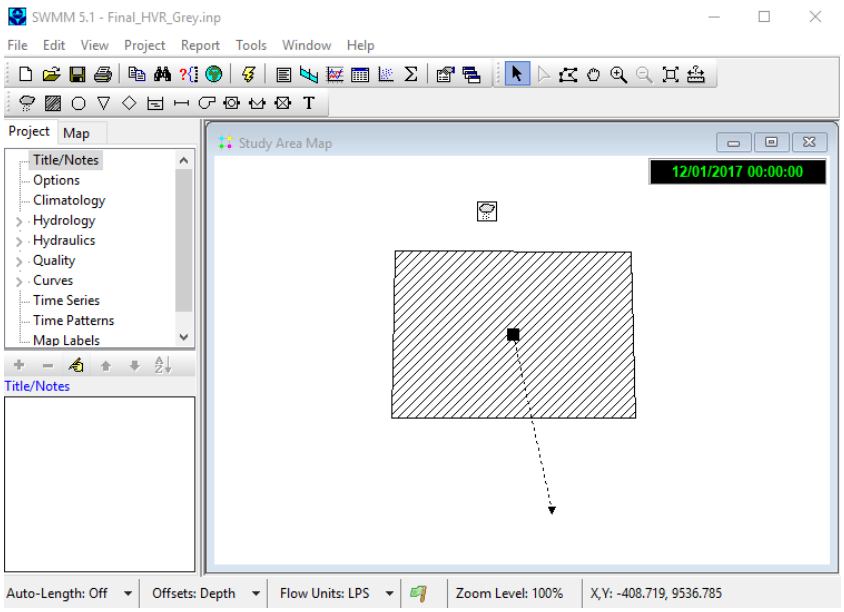

Figure A4.1. The grey roof model built up in SWMM with calibrated LID control

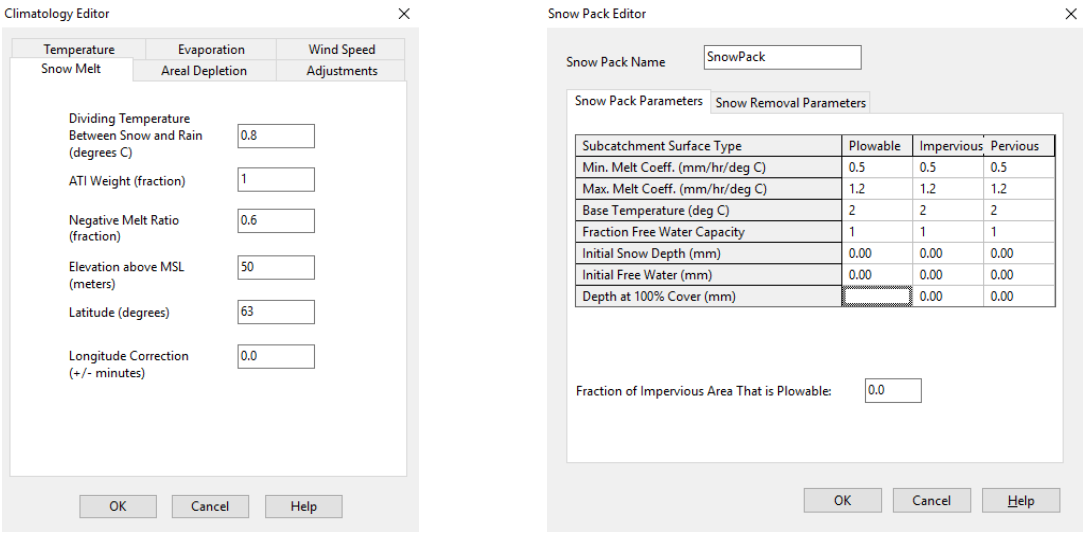

(a) **(b)**

Figure A4.2. Parameters to be calibrated in SWMM: (a) The snow-melt module; (b) The snowpack module.

Appendix 5 Matlab code

Matlab Script for implementing the entire conceptual model:

```
load('\\sambaad.stud.ntnu.no\lili\.profil\stud\datasal\Desktop\Masteroppgave\Matlab Model\Model of gray roof in winter\Input data\Winterperiod2017-8.mat')

%%Snow process

%Data source reading

timeSeries = SummaryTableFinal.Time_series(154081:349920);

Ta = SummaryTableFinal.Air_Temperature(154081:349920);

P = SummaryTableFinal.Precipitation_last_minute(154081:349920);

SR = SummaryTableFinal.Solar_radiation(154081:349920);

windSpeed = SummaryTableFinal.Wind_velocity(154081:349920);

airHum = SummaryTableFinal.Air_moisture(154081:349920);

obsR = SummaryTableFinal.Gray_roof_runoff(154081:349920);

Ts = SummaryTableFinal.Soil_Temperature_gray(154081:349920); %Soil Temperature


%Calibrating parameters in Snow pack process

beta1 = 6; %shortwave

beta2 = 1; %longwave

beta3 = 0.0001085; %latent heat

beta4 = 2.8; %sensible heat

beta5 = 9; %convective heat

Fr = 0.15; %Maximum fraction of water holding capacity in snow pack in weight

albedo = 0.9; %Snow albedo


%Calibrating parameters in ice-water heat exchange and roof model

beta6 = 600; %convective heat from leca

beta7=0.2; %convective heat from infiltrated water

beta8 = 4.5; %air sensible heat

upperSK = 1.5; %frozen hydraulic conductivity [m/min]

lowerSK = 0.68; %Unfrozen hydraulic conductivity [m/min]


 %Oberserved data

fc = 0.18; %Field capacity

Tmax = 1.5; %Temperature above which all precipitation is rain
```

```
Tmin = 1.2; %Temperature below which all precipitation is snow

%%Simulation of snow pack and runoff from snow pack
[snow, input] = snowProcess(Ta,P,SR,windSpeed,airHum,beta1,...
    beta2,beta3,beta4,beta5,Fr,Tmax,Tmin,albedo);

%%Ice-water heat exchange and Grey roof
duration = length(Ta);

%Configuration of the grey roof
width = 8; %Width[m]
lengt = 11; %Length[m]
depth = 200; %Depth[mm]
slope = 0.02; %Slope

%Properties of leca
poro = 0.55; %porosity
sk = 0.68; %Saturated hydraulic conductivity (No ice) [m/min]
rhoLeca = 500; %Bulk density of leca [kg/m3]

%Parameters for ice-water exchange
Li = 334000; %latent heat of freezing [J/kg]
rhoIce = 934; %Density of ice [kg/m3]
rhoWater = 1000; %Density of water [kg/m3]
Cair = 16700; %Melt rate of ice [J/kg*K]
%Specific heat content of water and ice [J/kg*K]
Cw = 4200;
Cice = 2108;

thetaWater = 0.09; %Initial Water content
thetaIce = 0.15; %Initial Ice content

%Simulated runoff
simR = zeros(duration,1); %Simulated runoff
```

```
for i = 1:(duration-1)
    %Temperature of incoming water
    if snow(i) < 2
        Tinput = 0;
    else
        Tinput = Ta(i);
    end

    thetaWater = thetaWater+input(i)/depth;

    %%Ice-water heat exchange
    Qsensible = Cleca*(Ts(i)-(-0.15));
    Qwater = 4.8*10^3*input(i)*(Tinput-(-0.15))*60;
    if snow(i) < 0.5 && Ta(i)>0
        QairSen = Cair*(Ta(i)-(-0.15));
    else
        QairSen = 0;
    end
    Qtotale = beta6*Qsensible+beta7*Qwater+beta8*QairSen;

    %Qm is the heat flow between snow and its contained water
    if Qtotale < 0 %net energy out
        Qm = min(-Qtotale,rhoWater*Li*1000*thetaWater*depth/1000);
    else %net energy in
        Qm = min(0,-(Qtotale-Cice*1000*thetaIce*depth/1000*(-1.5-Ts(i))));
    end

    %mass balance of the snow pack [mm]
    if Qm < 0    %melting
        deltaLiq = -max(Qm/(rhoWater*Li*1000*depth)*1000,-thetaIce);
        deltaIce = max(Qm/(rhoWater*Li*1000*depth)*1000,-thetaWater);
    else    %refreeze
        deltaLiq = -min(Qm/(rhoWater*Li*1000*depth)*1000,thetaIce);
        deltaIce = min(Qm/(rhoWater*Li*1000*depth)*1000,thetaWater);
    end
```

```
    thetaWater = max(0,thetaWater+deltaLiq);

    if thetaIce > 0.04
        sk = upperSK;
    elseif thetaIce<0.04 && thetaIce>0
        sk = (upperSK-lowerSK)/0.03*thetaIce+lowerSK;
    else
        sk = lowerSK;
    end

    if thetaWater < fc
        simR(i) = 0;
    else
        simR(i) = sk*width*(thetaWater-fc)*depth/poro*slope;
    end
    depH = simR(i)/(width*lengt);

    thetaIce = max(0,thetaIce+deltaIce);
    thetaWater = max(0,thetaWater-depH/depth);
end

NSE= NashCoefficient(simR,obsR);
error = errorOfRunoff(simR,obsR);

%The function is simulating snow accumulating and melting process
function [Wsnow,Runoff] = snowProcess(Ta,P,SR,windSpeed,airHum,...
    BETA1,BETA2,BETA3,BETA4,BETA5,FR,TMAX,TMIN,ALBEDO)

    rhoW = 1000;  %rhoW is density of water [kg/m3]
    cs = 2.108; %specific heat of ice [kJ/(kg*K)]
    namdaF = 333.6; %latent heat of fusion of snow [kJ/kg]
    deltaT = 1*60;
    duration = length(Ta);

    Wsnow = zeros(duration,1); % snow depth
```

```
    Wliq = zeros(duration,1); % water depth

    Psnow = 0; % Initial snow
    Prain = 0; % Initial rain

    Runoff = zeros(duration,1); %runoff from snow

    %snow accumulation and melt process
    for i = 1:(duration-1)
        %normal rain event
        if Ta(i) > TMAX
            Psnow = 0;
            if Wsnow(i) == 0
                Runoff(i) = P(i);
                continue;
            end
        %rain on snow
        elseif (Ta(i) <= TMAX && Ta(i) > TMIN)
                Psnow = (TMAX-Ta(i))/(TMAX-TMIN)*P(i);
        %pure snow
        else
            Psnow = P(i);
        end
        Prain = P(i) - Psnow;

        %saturated vapor pressure over water [hPa(100 Pa) or mb(millibar)]
        ew = (1.0007+(3.46*10^(-
6)*10^5))*6.1121*exp(17.502*Ta(i)/(240.97+Ta(i)));
        %saturated vapor pressure over ice [hPa(100 Pa) or mb(millibar)]
        ei = (1.0003+(4.18*10^(-
6)*10^5))*6.1115*exp(22.452*Ta(i)/(272.55+Ta(i)));
        %actual vapor pressure in the air
        ea = ew*airHum(i)/100;

        %snow surface temperature
        if Ta(i) > 0
```

```
    Ts = 0;
else
    Ts = Ta(i);
end

%Number of the day
if i <= 87840
    dayNum = 304+floor(i/60/24);
else
    dayNum = 1+floor((i-87840)/60/24);
end

sRad = shortwave(Wsnow(i), SR(i),ALBEDO,BETA1);
lRad = longwave(SR(i), Ta(i), Ts, dayNum, ea,BETA2);
lHeat = latentHeat(windSpeed(i), ea, ei,BETA3);
sHeat = sensibleHeat(lHeat, Ta(i), Ts, ea, ei,BETA4);
aHeat = advectedHeat(Prain, Ta(i),BETA5);

%Qnet < 0, net energy out
%Qnet > 0, net energy in
Qnet = (sRad+lRad+lHeat+sHeat+aHeat)*deltaT;

%Qm is the heat flow on snow phase change
if Qnet < 0
    Qm = min(-Qnet,rhoW*namdaF*1000*Wliq(i)/1000);
else
    Qm = min(0,-(Qnet-cs*1000*1000*Wsnow(i)/1000*(0-Ts)));
end

%mass balance of the snow pack [mm]
if Qm < 0    %melting
    deltaWliq = Prain-max(Qm/(rhoW*namdaF*1000)*1000,-Wsnow(i));
    deltaWsnow = Psnow+max(Qm/(rhoW*namdaF*1000)*1000,-Wliq(i));
else %refreeze
    deltaWliq = Prain-min(Qm/(rhoW*namdaF*1000)*1000,Wsnow(i));
    deltaWsnow = Psnow+min(Qm/(rhoW*namdaF*1000)*1000,Wliq(i));
```

```
        end
        Wsnow(i+1) = max(0,Wsnow(i)+deltaWsnow);
        Wliq(i+1) = max(0,min(Wliq(i)+deltaWliq,Wsnow(i+1)*FR));

        Runoff(i) = max(0, Wliq(i)+deltaWliq-Wsnow(i+1)*FR);
    end
end

function [ Qsw ] = shortwave( snowDepth, solRad, albedo,beta1 )
    depth = 5; %[mm]
    if snowDepth < depth %snow surface albedo
        A = snowDepth/10+0.4;
    else
        A = albedo;
    end

    if solRad > 0 %sola radiation
        Qsw = beta1*solRad * (1-A);
    else
        Qsw = 0;
    end
end

function [ Qlw ] = longwave( swr, Ta, Ts, dayNum, ea, beta2 )
    sigma = 5.67*10^(-8); %Stefan - Boltzmann constant [W/(m-2*K-4)]
    c = 2*3.1415*dayNum/365;
    Gex = 1366.1*(1.00011+(0.034221*cos(c))+(0.000128*sin(c))+(0.000719*...
        cos(2*c))+(0.000077*sin(2*c))); %extraterrestial radiation [W/m2]
    if swr > 0
        Nsquare = (1 - swr/Gex)/0.65;
    else
        Nsquare = 1.25;
    end
    K = 1 + 0.17*Nsquare;

    %net longwave
```

```
    Qlw = beta2*(K*sigma*(0.74+0.0049*ea)*Ta^4 - 0.98*sigma*Ts^4);
end

function [ Qe ] = latentHeat( wind, ea, ei,beta3)
    zt = 2;
    zb = 2;

    Qe = beta3*2359.9*8.5*0.673*2.24*(zt*zb)^(-1/6)*wind*(ea-ei);
end

function [ Qs ] = sensibleHeat( latentHeat, Ta, To, ea, eo,beta4 )
    gama = 0.00057*1000;

    Qs = beta4*latentHeat*gama*(Ta-To)/(ea-eo);
end

function [ Qp ] = advectedHeat( Px, Ta,beta5 )
    %Px: rainfall intensity (mm/s)
    Px = Px/60;

    Qp = beta5*4.8*10^3*Px*Ta;
end

function [ NC ] = NashCoefficient( s1, s2 )
%s1 is simulated runoff and s2 is observed runoff
    Aobs = mean(s2);
    lowerPart = 0;
    upperPart = 0;

    for i = 1:length(s1)
        upperPart = upperPart + (s1(i)-s2(i))^2;
        lowerPart = lowerPart + (s2(i)-Aobs)^2;
    end
    NC = 1-upperPart/lowerPart;
end
```

```
function [ eor ] = errorOfRunoff( s1, s2 )
%s1 is simulated runoff and s2 is observed runoff
    eor = (sum(s1)-sum(s2))/sum(s2);
end
```